



OPEN Effects and differences of various concentration techniques on the evolution of therapeutic components in Lushan geothermal water

Bo Zhang¹, Zheng Fang¹, Keng Xuan¹, Wenjie Ma¹, Bai Gao^{1,2✉}, Yuanyuan Liu¹, Dandan Huang¹, Silei Xie¹ & Yan Ding¹

Hot springs are significant geothermal resources characterized by their high mineral content and therapeutic value. This study aims to preserve the therapeutic element value of the Lushan hot springs in Jiangxi, China. Laboratory batch experiments, microstructural characterization, and hydrogeochemical modeling were employed to investigate the effects and differences of various concentration techniques under different environmental parameters on the evolution of therapeutic components in hot spring water. The key findings are as follows: Fluoride (F) concentrations in the hot spring water, along with elevated levels of iron (Fe) and manganese (Mn) observed at sampling point S2, exceed the World Health Organization (WHO) drinking water quality standards. Among the tested methods, atmospheric evaporation at 100 °C and pH = 4 demonstrated the highest concentration efficiency. Although freeze concentration achieved its best performance under −8 °C and pH = 6, its overall efficiency was still lower than that of atmospheric evaporation. However, freeze concentration requires low energy consumption and short processing cycles, making it a promising research direction for future hot spring concentration techniques. The evolution of potentially toxic elements revealed that arsenic (As) concentrations decreased during freeze concentration and remained below standard values at a freezing rate of 93.75%. In contrast, concentrations of chromium (Cr), manganese (Mn), and lead (Pb) exceeded permissible limits during atmospheric evaporation. SEM-EDS results showed differences in the microstructure of solid precipitates obtained from the two concentration methods. XPS analysis indicated that freeze concentration led to greater precipitation of potassium (K) and calcium (Ca) compared to atmospheric evaporation. PHREEQC simulations demonstrated that therapeutic components such as fluoride (F), lithium (Li), and strontium (Sr) primarily existed as single ions under both concentration methods, while silicon (Si) predominantly occurred as soluble SiO₂. This study provides green, diversified, and value-enhancing technological support for the sustainable development of geothermal resources in Lushan.

Keywords Hot springs, Concentration techniques, Therapeutic components, Evolution, Differences

Hot water and hot springs refer to natural fluids discharged from underground, with temperatures at least 4 °C above the local annual mean air temperature or exceeding the human core body temperature (37 °C). Scientifically, any spring water with a temperature higher than the local groundwater temperature qualifies as a hot spring¹. As an essential geothermal resource, hot springs are characterized by high water temperatures, significant mineralization, and the presence of elements such as sulfur, calcium, and magnesium. These properties contribute to therapeutic effects, including skin improvement, muscle fatigue relief, and enhanced blood circulation². Hot springs are primarily distributed in tectonically active regions, such as volcanic zones and fault areas, where they exert unique ecological and environmental impacts³; they hold significant potential for applications in healthcare, tourism, and energy sectors.

¹School of Water Resources & Environmental Engineering, East China University of Technology, Nanchang 330013, China. ²State Key Laboratory of Nuclear Resources and Environment, East China University of Technology, Nanchang 330013, China. ✉email: gaobai@ecit.cn

The therapeutic and health benefits of hot springs have garnered significant attention and research from scholars worldwide, particularly regarding the characteristics of their therapeutic components. Fluoride (F) is one of the essential trace elements for the human body. An appropriate intake of fluoride promotes the utilization and deposition of calcium and phosphorus in bones, accelerating bone formation and enhancing bone density. Fluoride has also been proven to be the only nutrient that reduces the incidence and severity of dental caries in both children and adults⁴. According to the World Health Organization⁵ the guideline value for fluoride in drinking water is 1.5 mg/L, and excessive intake may pose health risks. However, it should be noted that the hot spring water in this study is intended primarily for external therapeutic use, such as bathing. The slightly higher concentrations of fluoride may be beneficial in external treatments, especially for joint and skin-related disorders⁶. Metasilicic acid (H_2SiO_3) has a softening effect on aortic sclerosis and provides therapeutic benefits for heart disease, hypertension, arteriosclerosis, neurological disorders, gastritis, and gastric ulcers⁷. Although the term metasilicic acid is often used in earlier literature, it is now recognized that orthosilicic acid (H_4SiO_4) is the predominant soluble form of silica in natural waters and responsible for the therapeutic effects attributed to silica⁸. Iron is an essential component for oxygen transport and exchange in human blood. Lithium helps regulate central nervous system activity and boosts immune function, while strontium strengthens bones and prevents cardiovascular diseases. Bromine can suppress central nervous system excitement, providing a calming effect⁹. Numerous studies on the therapeutic components of hot springs indicate that the human body experiences synergistic physical and chemical effects during hot spring bathing. For instance, Naima Farhat et al.¹⁰ observed that the temperature of hot spring water promotes oxygen flow within body tissues, dilates the skin, and increases the flow rate of sedative substances, thereby relaxing muscles. Yang Bei et al.¹¹ found through controlled experiments and statistical analysis that hot springs effectively alleviate mental stress in sub-healthy individuals, improve sleep quality, and potentially offer therapeutic benefits for obesity. Similarly, Phurpa Wangchuk et al.¹² conducted a comprehensive analysis of hot spring therapy cases from countries including Thailand, Japan, Indonesia, and China. They concluded that hot springs facilitate the direct absorption of minerals such as calcium, iron, magnesium, potassium, sodium, and silica through the skin, aiding in the treatment of skin conditions like atopic dermatitis and psoriasis. Recently, Sheng Lili et al.¹³ leveraged the properties of hot springs to promote blood circulation and angiogenesis. They designed a novel bioactive photothermal hydrogel with a “hot spring effect,” using siderite and carboxymethyl chitosan (NOCS) as raw materials. This hydrogel releases bioactive ions and creates a thermal ionic environment at wound sites, significantly enhancing angiogenesis and chronic wound healing *in vivo*.

Although hot spring water contains components with notable therapeutic effects, these are primarily trace elements with low concentrations, making their effective utilization challenging. With growing recognition and demand for the therapeutic efficacy of hot spring water, concentration techniques have been widely studied as an effective method for extracting valuable elements from it. Concentration techniques involve the removal of part of the solvent from a target solution through various methods, thereby increasing the concentration of the remaining solution. In recent years, advancements in concentration technology have facilitated its widespread application in fields such as food processing, environmental protection, and healthcare^{14–16}. For instance, Orellana et al.¹⁷ employed freeze concentration to study bioactive compounds in apple juice and found that phenolic compounds increased by 1.9, 2.9, and 3.8 times in three freeze concentration stages, respectively. This demonstrated that freeze concentration can enhance the phenolic compound content, thereby improving the antioxidant activity, sensory qualities, nutritional value, and antioxidative properties of apple juice. Similarly, Alizadeh et al.¹⁸ utilized atmospheric evaporation techniques to preserve key quality traits in bayberry juice. Šir and Honzajková¹⁹ applied continuous evaporation to minimize residual waste volume, enabling the recovery of trace elements from waste. Despite the maturation and broad application of concentration technologies, maximizing the preservation of therapeutic elements in hot spring water remains an area of exploration. This study aims to provide innovative insights into the application of traditional concentration techniques for hot spring water, paving the way for future advancements in this field.

However, the naturally occurring concentrations of certain therapeutic constituents in geothermal water are often below the thresholds required for effective medical or balneological use, thereby necessitating the implementation of enhancement techniques²⁰. To address this, physical concentration methods such as evaporation and freeze concentration are explored as effective, non-chemical strategies to increase the content of key therapeutic elements (e.g., H_4SiO_4 , Sr^{2+} , Li^+) while maintaining the physicochemical integrity and natural composition of the geothermal water. These approaches can support the development of standardized therapeutic formulations, especially for regions lacking direct access to geothermal resources.

The Lushan hot springs are located in the Lushan Mountain range of Jiangxi Province, China, at the junction of the Jiangnan anticline and the Lower Yangtze depression, an area characterized by complex geological structures. The region is predominantly composed of metamorphic rocks from the Precambrian and sedimentary rocks from the Sinian period, accompanied by igneous rocks from the Early Cretaceous and Neoproterozoic eras, such as the Yujingshan monzogranite and Guanyinqiao granitic gneiss. Intrusive rocks, primarily granitic pegmatites, are well-developed, with faults mainly trending in an east-west direction and exhibiting high density and large scale. The hot spring water maintains a consistent temperature of 40–50 °C throughout the year and is rich in Fe, Li, Sr, Br, F, and H_4SiO_4 , offering significant potential medical value with beneficial effects on human health^{21,22}. However, the current utilization of the Lushan hot springs is primarily focused on bathing and therapeutic recreation, resulting in substantial water consumption and underutilization of their economic potential. By applying concentration techniques to the natural hot spring water, therapeutic components could be concentrated through specific processes, transforming the resource into a small-volume, high-value product. This approach would enable diversified applications of the hot springs, maximize their utilization potential, and address the current issues of resource wastage and low efficiency. Furthermore, it would facilitate resource sharing and contribute to the sustainable development of geothermal resources.

Reagent Name	Chemical formula	Quality	Manufacturer	Applications
Nitric acid	HNO ₃	AR	Xilong Chemical Co.	Field sample preservative
Sodium hydroxide	NaOH	AR	Xilong Chemical Co.	pH adjustment
Hydrochloric acid	HCl	AR	Xilong Chemical Co.	pH adjustment
Iron standard solution	Fe(NO ₃) ₂	AR	National Center for Nonferrous Metals Analysis and Testing	Standard solution for analytical testing
Lithium standard solution	Li(NO ₃) ₂	AR	National Center for Nonferrous Metals Analysis and Testing	Standard solution for analytical testing
Strontium standard solution	Sr(NO ₃) ₂	AR	National Center for Nonferrous Metals Analysis and Testing	Standard solution for analytical testing
Silicon standard solution	SiO ₂	AR	Tanmo Center for Quality Assurance Standards	Standard solution for analytical testing
Fluorine standard solution	NaF	AR	National Center for Nonferrous Metals Analysis and Testing	Standard solution for analytical testing

Table 1. Experimental principal reagent. Note: AR stands for Analytical Reagent grade.

Name of Instrument	Model number
Ultrapure water machine	Smart-Q30(Shanghai Hantai Instrument Co., Ltd)
Multi-parameter water quality tester	HQ40D(Hach Company, USA)
Probe-type digital thermometer	MIK-TP101(Shenzhen GaoDe Electronics Co., Ltd.)
Low-temperature thermostatic bath	DFY-5 L-20(Gongyi Yuhua Instrument Co., Ltd.)
Constant temperature water bath	78HW-1(Changzhou Guoyu Instrument Manufacturing Co., Ltd.)
Electronic Analytical Balance	AR224 CN (OHAUS Instruments (Shanghai) Co., Ltd.)
Ultrasonic cleaner	F-100 S(Shenzhen Foyom Technology Group Co., Ltd.)
Temperature-controlled refrigerator	HYC-650(Haier)
Freeze dryer	FD-1 A-50(Shanghai Yuming Instrument Co., Ltd.)
Inductively Coupled Plasma Emission Spectrometer	Agilent 5100 ICP-OES
Ion Chromatograph	ICS-1100
Flame atomic absorption spectrophotometry	AAS6000
FTIR spectrometer	Thermo Scientific Nicolet iS5
Field Emission Scanning Electron Microscopy	TESCAN MIRA LMS
X-ray photoelectron spectrometer	Thermo Scientific ESCALAB Xi+

Table 2. List of major instruments and equipment.

This study focuses on the Lushan hot springs, investigating their concentration characteristics under two commonly used concentration techniques: freeze concentration and atmospheric evaporation. Through controlled experiments (e.g., temperature and pH conditions), the effects of various influencing factors on the concentration of therapeutic components (Fe, Li, Sr, Br, F, and H₄SiO₄) in the hot spring water were examined. Additionally, the study explored the evolution of potentially toxic elements in hot spring water during the two concentration processes. Microscopic characterization techniques, including SEM-EDS, XPS, and FT-IR, were employed to analyze the solid precipitates formed during concentration, providing preliminary insights into their concentration and evolution characteristics. The two concentration methods were further compared in terms of their concentration efficiency and economic value. Given the significant economic and societal importance of hot spring water concentration, this research aims to provide green, diversified, and high-value technical solutions for the sustainable development of Lushan's geothermal resources.

Materials and methods
Experimental reagents and instruments

Experimental reagents
The reagents required during the experimental process include those used for measuring water quality indicators during field surveys, reagents for hot spring water concentration experiments, and reagents for hydrochemical analysis and testing. The main reagents used in the experiments are listed in Table 1.

Experimental instruments
The main instruments and equipment used in the experimental process are listed in Table 2.

Experimental methods
Sample collection

In this study, field sampling was conducted on four hot springs (S1–S4) from the Xingzi hot springs in Lushan, Jiangxi Province. The drilling depths of the S1–S4 hot springs were 238 m, 486 m, 206 m, and 524 m, respectively. The distribution of sampling points and field conditions are shown in Fig. 1. Samples were collected using polyethylene bottles of different specifications. Prior to sampling, the bottles were rinsed and soaked three times with the target hot spring water to minimize contamination. Care was taken to avoid introducing external

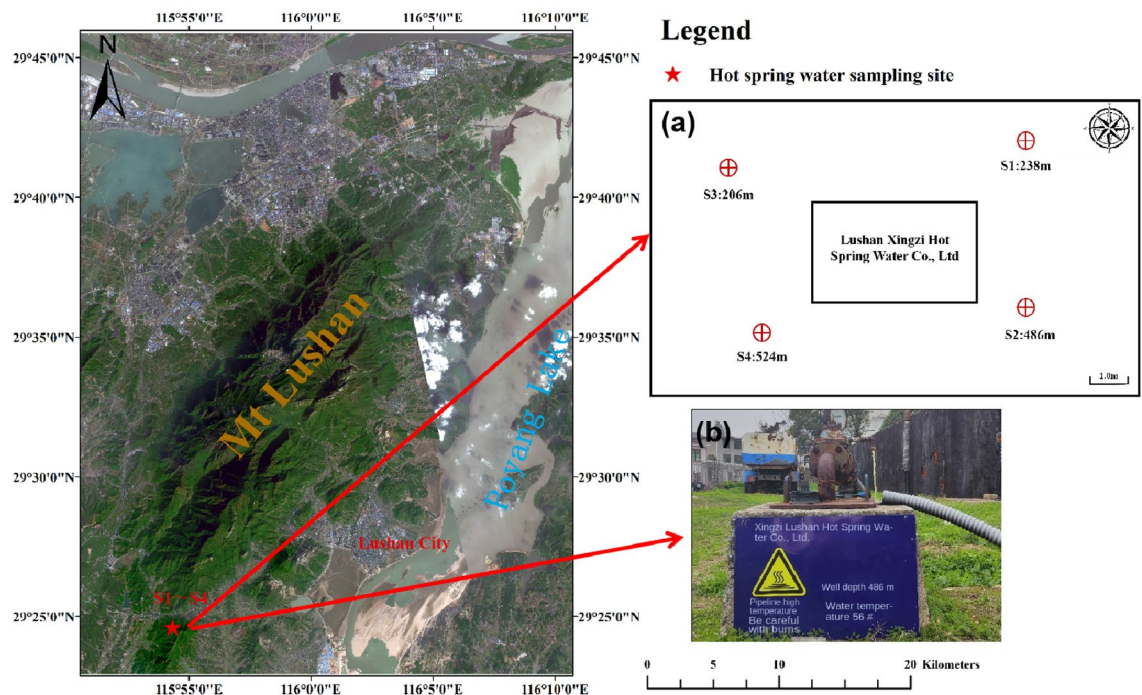


Fig. 1. Map of sampling sites in the study area. (a) The figure shows the distribution of sampling sites in the study area; (b) Photograph of core samples from the hot spring borehole; Note: The map was independently created by the authors using ArcGIS 10.7 (<https://www.esri.com/zh-cn/about/about-esri/company>), and there are no copyright issues associated with its use. Figure 1 (a) was produced by the authors using WPS Presentation (Version 12.1.0.20784, Kingsoft, <https://platform.wps.cn/>), and Fig. 1 (b) is an original field photograph.

pollutants during sampling. The bottles were filled completely with hot spring water, ensuring overflow to expel any air, and were sealed with waterproof film to prevent air intrusion.

Concentration experiment

Selected hot spring water with therapeutic value was used for concentration experiments to investigate the effects and differences of various environmental parameters on the evolution of therapeutic components in the hot spring water.

(1) Atmospheric Evaporation Concentration Experiment.

A 500 mL sample of Lushan hot spring water was placed in a beaker, which was then positioned in a water-oil bath and subjected to atmospheric evaporation according to the experimental conditions. The hot spring water was stirred magnetically and heated until it reached a specific volume (evaporation rates of 50%, 75%, 83.3%, 87.5%, 93.75%, and 96.875%). During the evaporation process, the pH, Eh, and temperature of the hot spring water were measured using a thermometer and a multi-parameter measuring instrument. In this study, a 3 mL liquid sample was filtered using a 0.45 µm pore-size water-based filter membrane to analyze the therapeutic components and heavy metal elements in the hot spring water, following the Standard Methods for the Examination of Water and Wastewater, 24th Edition (Baird et al., 2017). Finally, the precipitated solid was dried, weighed, and sealed for storage, and phase analysis was performed in subsequent steps.

① Effect of Temperature on Hot Spring Concentration: The experimental environment temperature was maintained at $25\text{ °C} \pm 0.5\text{ °C}$, with a magnetic stirring speed of 200 r/min. The water bath temperature was set to $80\text{ °C} \pm 0.5\text{ °C}$, $100\text{ °C} \pm 0.5\text{ °C}$, $120\text{ °C} \pm 0.5\text{ °C}$, and $140\text{ °C} \pm 0.5\text{ °C}$.

② Effect of pH on Hot Spring Concentration: The experimental environment temperature was maintained at $25\text{ °C} \pm 0.5\text{ °C}$, with a magnetic stirring speed of 200 r/min. The pH of the hot spring water was adjusted to 4 ± 0.1 , 6 ± 0.1 , and 8 ± 0.1 using 0.1 M HCl and 0.1 M NaOH. The experiment was conducted under optimal temperature conditions. The best experimental conditions were determined based on the single-factor experiments.

(2) Freeze Concentration Experiment.

A 500 mL sample of Lushan hot spring water was placed in a beaker, which was then positioned in a low-temperature constant temperature bath. Ethylene glycol was used as the cooling transfer medium, and progressive freeze concentration was performed according to the experimental conditions. Thin ice formed on the beaker walls at regular intervals, and the beaker was removed, allowed to stand, and the thin ice was scraped off. Once



Fig. 2. Photograph of the freeze concentration experimental apparatus.

Analytical Test Items	Methods of analysis	Standard Methods Code
Fe	Flame atomic absorption spectrophotometry	APHA Standard Method 3111 B
Li	Flame atomic absorption spectrophotometry	APHA Standard Method 3111 B
Sr	Flame atomic absorption spectrophotometry	APHA Standard Method 3111 B
H ₄ SiO ₄	Ammonium molybdate spectrophotometric	APHA Standard Method 4500-Si B
As、Cd、Cr、Cu、Mn、Ni、Pb、Se、Zn	Plasma emission spectroscopy	APHA Standard Method 3120 B
Br ⁻	Ion chromatography	APHA Standard Method 4110 B
F ⁻	Ion chromatography	APHA Standard Method 4110 B
HCO ₃ ⁻	Acid-base titration	APHA Standard Method 2320 B
pH	Multi-Parameter Measuring Instrument	APHA Standard Method 4500-H ⁺
Eh	Multi-Parameter Measuring Instrument	APHA Standard Method 2580 B
Temperature	Thermometer	APHA Standard Method 2550 B

Table 3. Main water chemical index analysis test items and methods. Note: The instruments used for analytical testing are the same as those listed in Table 2. Both pH and Eh measurements were conducted with automatic temperature compensation. The reported Eh values have been calibrated against the Standard Hydrogen Electrode (SHE), thus reflecting the true redox potential (in mv) of the hot spring water samples.

the hot spring water reached a specific volume, the remaining steps were the same as those in the atmospheric evaporation experiment.

① Effect of Temperature on Hot Spring Concentration: The experimental environment temperature was maintained at 25 °C ± 0.5 °C, with a magnetic stirring speed of 200 r/min. The temperature of the low-temperature constant temperature bath was set to −8 °C ± 0.1 °C, −12 °C ± 0.1 °C, and −16 °C ± 0.1 °C.

② Effect of pH on Hot Spring Concentration: The experimental environment temperature was maintained at 25 °C ± 0.5 °C, with a magnetic stirring speed of 200 r/min. The pH of the hot spring water was adjusted to 4 ± 0.1, 6 ± 0.1, and 8 ± 0.1 using 0.1 M HCl and 0.1 M NaOH. Prior to the freeze-drying experiments, each hot spring water sample was adjusted to the target pH value. After adjustment, the samples were directly subjected to freeze-drying without further pH modification during the process. The actual apparatus used for the freeze concentration experiment is shown in Fig. 2. During the freeze-drying process, no further pH modification was possible due to the closed system. The experiment was conducted under optimal temperature conditions. The best experimental conditions were determined based on the single-factor experiments.

Analytical test methods

In this study, 10–20% of the test samples were randomly selected for parallel duplicate testing and spike recovery analysis. For each batch of samples with the same matrix, the same analyses were performed. The main hydrochemical indicators and analysis methods are listed in Table 3²³.

To verify the overall analytical accuracy, the cation-anion charge balance was calculated for the hot spring water samples, and all values were within the acceptable range ($\pm 5\%$), indicating satisfactory charge balance. The calculation formula for Ion Balance (IB) is as follows:

$$ib = \frac{(\sum \text{cation} - \sum \text{negative ion})}{(\sum \text{cation} + \sum \text{negative ion})} \times 100\% \quad (1)$$

In this study, the surface of the precipitated solids was microscopically imaged using the Czech TESCAN MIRA LMS field emission scanning electron microscope (SEM). The elemental composition and mass ratio of elements in the precipitated solids were analyzed using the Energy Dispersive Spectrometer (EDS) on the American Escalab 250Xi X-ray photoelectron spectrometer. The elemental composition and chemical states of the precipitated solids were further analyzed using the X-ray photoelectron spectroscopy (XPS) on the American Thermo Scientific ESCALAB Xi + system.

Data processing

In this study, Excel 2016 was mainly used for data preprocessing, and statistical analysis was performed using SPSS 24.0. The Piper tri-linear diagram, concentration process curves, and other figures in this paper were generated using PHREEQC, Origin 2017, and AquaChem40 software.

(1) Calculation Method for the Concentration Factor (K) of Hydrochemical Components During the Concentration Experiment: The concentration factor (K) was calculated using the formula shown in Eq. 1:

$$K = \frac{C_2}{C_1} \times 100\% \quad (2)$$

In the equation: K - Concentration factor, dimensionless; C_1 - Initial concentration of the hydrochemical component, mg/L; C_2 - Concentration of the hydrochemical component after concentration, mg/L.

(2) Calculation Method for the Evaporation/Freezing Rate of Hot Spring Water During the Concentration Experiment: The evaporation/freezing rate was calculated using the formula shown in Eq. 2:

$$R = 1 - \frac{V_2}{V_1} \times 100\% \quad (3)$$

In the equation: R - Evaporation/freezing rate of hot spring water, %; V_1 - Initial volume of water, mL; V_2 - Current volume of water, mL.

(3) Acidification Before Hydrochemical Analysis: Acidification before hydrochemical analysis can cause dilution of the solution. To accurately determine the ion concentration, the true values need to be back-calculated based on the test results. The calculation method is shown in Eq. 3:

$$C = C_1 \times \frac{V_2}{V_1} \times 100\% \quad (4)$$

In the equation: C - Actual ion concentration, mg/L; C_1 - Ion concentration measured by the instrument, mg/L; V_1 - Volume of water sample, mL; V_2 - Volume of the acidified sample, mL.

PHREEQC, developed by the United States Geological Survey (USGS), is a geochemical modeling software widely used for calculations of water-chemical equilibrium, water-rock interactions, speciation of aqueous components, and mineral saturation index analysis. It supports various thermodynamic databases and is applicable to studies of groundwater evolution, contaminant transport, and resource utilization²⁴.

The Ilnl database bundled with PHREEQC Version 3 was selected for this study. By running the PHREEQC software, the speciation and concentration of chemical components in the hot spring water at different concentration stages were obtained. Based on the output data, the effects of the concentration processes on the speciation of therapeutic components in the hot spring water were analyzed.

Input parameter settings:

In the experimental processes, both freeze concentration and atmospheric evaporation samples were analyzed for major cations and anions. The input parameters used for simulating the speciation of therapeutic components correspond to the measured data at different stages of concentration for each method.

- (1) Therapeutic components: Due to the fact that Fe was almost undetectable during the concentration experiments and Br existed only in the form of Br^- , the simulated therapeutic components during the hot spring water evolution process were limited to Li, Sr, F, and H_4SiO_4 . Their concentrations were based on on-site measurements during the experiments.
- (2) Major cations and anions: The simulation of hot spring water evolution involved the following major ions: Li, Sr, Si, F, Cl^- , SO_4^{2-} , and HCO_3^- , all of which were determined through on-site measurements.
- (3) Temperature: The temperatures used in the simulation were all based on field-measured data during the experiments and are reported in degrees Celsius.
- (4) pH: All pH values used in the speciation modeling were directly measured during the experimental processes.
- (5) pe value: The pe value, which reflects the electron activity at equilibrium, can be derived from the redox potential (Eh). In this study, Eh values were measured in the field, and the pe values used in the simulation were calculated based on the following relationship between Eh and pe:

samples	temperature/℃	TDS /mg·L ⁻¹	Eh /mv	pH	Na ⁺	K ⁺	Mg ²⁺	Ca ²⁺	Cl ⁻	SO ₄ ²⁻	HCO ₃ ⁻	CO ₃ ²⁻	Ib/%
					mg·L ⁻¹								
S1	77.9	450	-78.5	8.2	90.9	2.9	0.4	5.8	8.49	16.54	113.73	4.50	2.23
S2	55.0	342	-6.8	8.1	20.4	2.6	13.9	34.7	9.67	14.57	125.93	0	1.38
S3	64.4	435	-5	8.38	86.5	2.9	0.8	9.0	8.10	16.48	115.26	9.00	2.37
S4	77.2	440	-97.3	8.51	94.8	2.7	0.1	3.0	10.19	12.53	113.73	4.50	2.87

Table 4. Chemical analysis of Lushan spring Water.

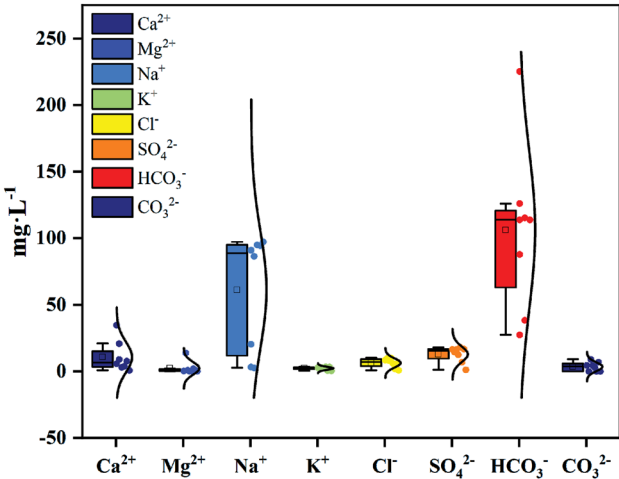


Fig. 3. Box diagrams of chemical parameters of Lushan hot spring water.

$$pe = \frac{nF}{2.303RT} \times Eh \tag{5}$$

Where: pe - the logarithmic expression of the electron activity, commonly used as an indicator of redox reaction intensity; n - the number of electrons involved in the redox reaction; F - Faraday constant, taken as 96,485 C/mol in this study; R - universal gas constant, taken as 8.314 J/(mol·K) in this study; T - temperature in Kelvin, taken as 298 K in this study; Eh - redox potential in millivolts (mV).

Results and discussion
Hydrogeochemistry of hot spring water

Main dissolved constituents
The composition of main dissolved constituents and physicochemical parameters of Lushan hot spring water are summarized in Table 4; Fig. 3. The concentrations of cations, including Ca²⁺, Mg²⁺, Na⁺, and K⁺, ranged from 3.0 to 34.70, 0.10 to 13.90, 20.4 to 94.8, and 2.6 to 2.9 mg·L⁻¹, respectively, with average values of 13.12, 3.8, 73.15, and 2.78 mg·L⁻¹. The concentrations of anions, including HCO₃⁻, Cl⁻, and SO₄²⁻, ranged from 27.46 to 225.15, 0.02 to 16.49, and 0.80 to 10.19, and 1.23 to 18.00 mg·L⁻¹, respectively, with average values of 105.93, 8.21, 6.37, and 12.88 mg·L⁻¹. The physical properties of the hot spring water are colorless and transparent, with some springs exhibiting a distinct sulfur odor. The water temperature ranges from 55.0 to 77.9 °C, and the pH ranges from 8.1 to 8.8, indicating that the water is neutral to weakly alkaline. The total dissolved solids (TDS) range from 342 to 450 mg·L⁻¹, classifying the water as fresh. The primary water chemistry type is HCO₃-Na type (Fig. 4).

Based on the results of the correlation coefficient heat map (Fig. 5), the enrichment of F⁻ in the study area is significantly positively correlated with H₄SiO₄ (*r* = 0.96) and Li (*r* = 0.89), suggesting that its source is controlled by the hydrolysis of silicate minerals (such as biotite and amphibole). The alkaline environment (pH, *r* = 0.89) and high-temperature conditions (temperature, *r* = 0.92) jointly promote the dissolution of fluorine-bearing minerals. The perfect collinearity of Li⁺ with TDS (*r* = 0.99) and Na⁺ (*r* = 1.00) indicates that evaporative concentration dominates its migration, while the strong correlation between Li and H₄SiO₄ (*r* = 0.97) further supports the contribution of weathered lithium silicate minerals. The co-variation of Sr²⁺ with Ca²⁺ (*r* = 0.98), Mg²⁺ (*r* = 0.96), and HCO₃⁻ (*r* = 0.97) reveals that the dissolution of carbonate minerals is its main source, and the positive correlation with Eh (*r* = 0.76) may reflect that the acidic environment driven by the oxidation of sulfides under oxidizing conditions accelerates the release of Sr²⁺. The concentration of H₄SiO₄ is simultaneously controlled by the intensity of water-rock interaction (TDS, *r* = 0.93; temperature, *r* = 0.90) and redox conditions (Eh, *r* = -0.75). Although SO₄²⁻ and Cl⁻ are the dominant anions in the spring water, their correlation with

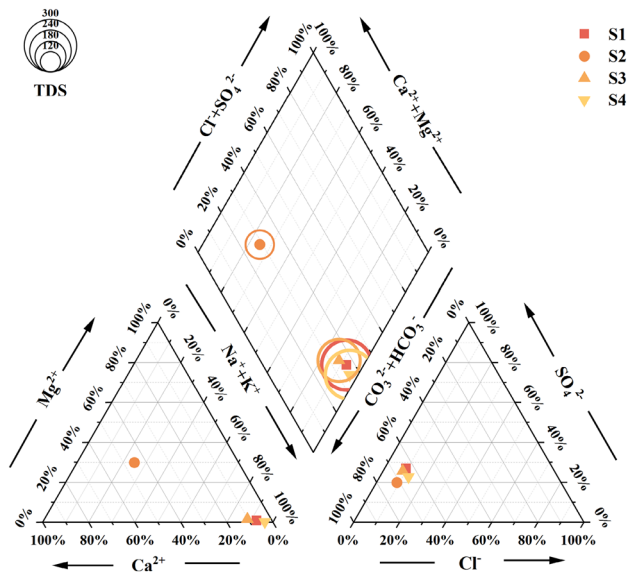
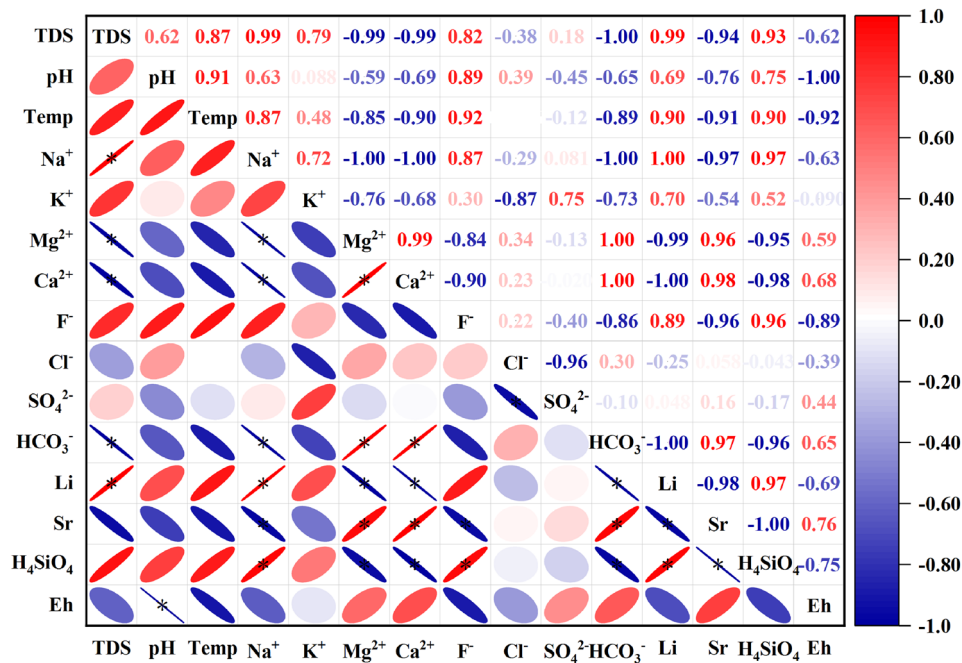


Fig. 4. Piper diagram of hot spring in Lushan.



* p<=0.05

Fig. 5. Correlation of water chemical components.

therapeutic components such as Li, Si, F, and Sr is relatively low, indicating that they have a limited impact on the concentration behavior of these components.

Physical therapy components

The therapeutic components in Lushan hot spring water primarily include Fe, Li, Sr, Br, F, and H₄SiO₄. These hydrochemical components have been reported to have beneficial effects on human health in current studies, and their concentrations are shown in Table 5.

- (1) In this study, the concentrations of F in the S1, S3, and S4 hot springs were 7.54, 5.56, and 10.72 mg/L, respectively, all values exceed the WHO guideline limit for fluoride (1.5 mg/L)⁵. According to the “Geothermal Resources Geological Survey Code (GB11615-2010, China)” for the classification of therapeutic

samples	S1	S2	S3	S4	WHO standards
Fe	0.09	2.09	0.21	0.03	0.3
Mn	0.02	0.30	0.02	ND	0.08
Li	0.142	0.058	0.130	0.146	/
Sr	0.053	0.108	0.060	0.036	/
Br	1.159	1.168	1.125	1.127	/
F	7.54	1.98	5.56	10.27	1.5
H ₄ SiO ₄	70.65	58.48	69.42	74.96	/
As	ND	ND	ND	ND	0.01
Cd	ND	ND	ND	ND	0.003
Cr	ND	ND	ND	ND	0.05
Cu	ND	0.001	ND	ND	2.0
Ni	ND	0.001	ND	ND	0.07
Pb	ND	0.001	ND	ND	0.01
Se	ND	ND	ND	ND	0.04
Zn	ND	0.01	ND	ND	3.0

Table 5. Test results of other ionic components. Note: “ND” denotes “not detected.” All units in the table are expressed in mg/L. “/” denotes “unlimited value.”

mineral waters (concentration > 2 mg/L), the S1, S3, and S4 hot springs are classified as fluoride-rich waters, which are expected to have the aforementioned positive effects on human health.

- (2) The variation in H₄SiO₄ content is mainly influenced by leaching and hydrolysis processes²⁵. The concentrations of H₄SiO₄ in the S1, S3, S4 hot spring waters were 70.65, 58.48, 69.42, and 74.96 mg/L, respectively, which meet the threshold of mineral water concentration (> 50 mg/L) as per the “Geothermal Resources Geological Survey Code (GB11615-2010, China),” indicating that H₄SiO₄ in Lushan hot springs possesses significant therapeutic potential.
- (3) Fe, Li, Sr, and Br are present in the S1 to S4 hot springs of Lushan. The concentrations of these four therapeutic components, ranging from 0.03 to 2.09 mg/L (Fe), 0.058 to 0.146 mg/L (Li), 0.036 to 0.108 mg/L (Sr), and 1.13 to 1.68 mg/L (Br), do not meet the threshold for therapeutic mineral water concentration defined in the “Geothermal Resources Geological Survey Code (GB11615-2010, China),” and therefore, their therapeutic effects on human health are relatively minor. Moreover, the concentrations of Fe and Mn at sampling point S2 exceed the limits set by the World Health Organization (WHO)⁵ for drinking water.

Study of freezing concentration

Effect of temperature

Temperature is a key factor affecting the efficiency of the concentration process, as it directly influences the solubility of solutes and the evaporation rate in the solution, thereby impacting the overall concentration performance²⁶. Accurate temperature control is therefore essential during the concentration process to balance efficiency and quality. Based on the concentrations and freezing points of therapeutic components in Lushan hot spring water, the S1 spring was selected as a representative sample for the concentration experiment. The freeze concentration process was conducted under three temperature gradients: −8 °C, −12 °C, and −16 °C. The effect of temperature on the freeze concentration of therapeutic components in Lushan hot spring water was investigated, and the results are presented in Fig. 6.

From the results shown in Fig. 6, at −8 °C, the concentrations of Li, Sr, F, Br, and H₄SiO₄ in the spring water reached 0.59 mg/L, 0.13 mg/L, 28.19 mg/L, 1.29 mg/L, and 212.86 mg/L, respectively. The corresponding concentration factors were 3.64, 4.27, 3.74, 1.11, and 2.90. During the initial freezing ratio stage (0–50%), the concentration of H₄SiO₄ increased significantly, while in the later stage (50–93.75%), it exhibited a gradual and uniform increase. After concentration, the F and H₄SiO₄ contents reached 14.09 and 4.26 times their standard values, respectively (Fig. 7). At −12 °C, the Li concentration increased from 0.16 mg/L to 0.59 mg/L, Sr from 0.16 mg/L to 0.43 mg/L, F from 7.54 mg/L to 21.85 mg/L, Br from 1.16 mg/L to 1.25 mg/L, and H₄SiO₄ from 73.38 mg/L to 152.99 mg/L. The respective concentration factors were 2.69, 3.09, 2.90, 1.08, and 2.08. Before the freezing ratio reached 83.3%, the H₄SiO₄ concentration increased rapidly; however, beyond this point, the rate of increase slowed. After concentration, the F and H₄SiO₄ contents were 10.93 and 3.06 times their standard values, respectively (Fig. 7). At −16 °C, the concentration factors for Li, Sr, F, Br, and H₄SiO₄ were 2.23, 1.82, 2.63, 2.52, and 1.82, respectively. During the freezing ratio stage of 87.5–93.75%, the change in H₄SiO₄ concentration was minimal. After concentration, the F and H₄SiO₄ contents were 9.49 and 2.67 times their standard values, respectively (Fig. 7).

The optimal temperature for the freeze concentration of therapeutic components was determined to be −8 °C. During the freeze concentration process, the pH of the spring water gradually decreased from an initial value of 8.72 to a range of 8.11–8.33. Fe was not detected (concentration remained below the detection limit of 0 mg/L throughout the experiment), although it was retained in Fig. 6 for completeness. In contrast, Li, Sr, and Br were concentrated to some extent but still did not reach the therapeutic concentration thresholds required for medicinal thermal mineral water. Overall, although freeze concentration could enhance the therapeutic

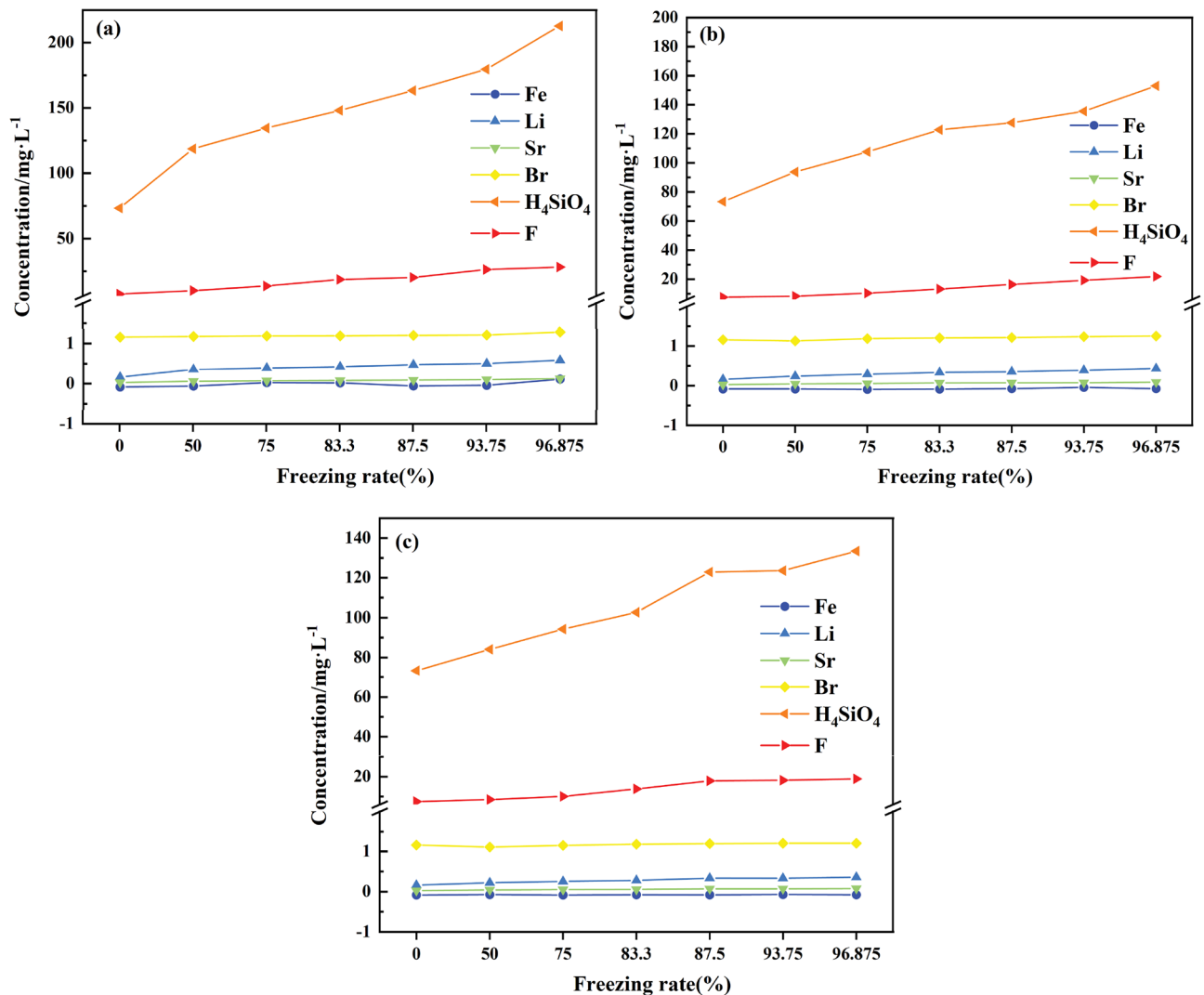


Fig. 6. Effect of temperature on freezing concentration of valuable elements of Lushan hot Spring physiotherapy: (a) Freezing temperature -8°C ; (b) Freezing temperature -12°C ; (c) Freezing temperature -16°C .

components in the spring water, the concentration effect was suboptimal due to a high degree of solute entrapment. This phenomenon occurs when water molecules condense into ice crystals, trapping or adhering solutes on the crystal surfaces²⁷.

Two primary factors likely contributed to this outcome. Firstly, freezing temperature affects both nucleation and ice crystal growth. The balance between these processes varies at different temperatures, and the concentration of solutes in the solution influences their escape during freezing. Higher solute concentrations in the solution result in greater sensitivity to freezing temperatures, thereby reducing the efficiency of solute exclusion from ice crystals²⁸. Secondly, at the solid-liquid interface, water molecules crystallize under the influence of hydrogen bonding, releasing solutes from the growing ice crystals. A concentration gradient exists between the solid-liquid interface and the bulk solution, causing water molecules to move toward the interface while solute molecules diffuse into the liquid phase. Lower freezing temperatures result in slower ice crystal growth, which reduces solute entrapment within the ice crystals (Fig. 8). Consequently, the concentration efficiency improves at lower freezing temperatures²⁹.

Effect of initial pH

The variation in pH significantly affects the speciation and solubility of dissolved minerals in water. For instance, lower pH values may promote the dissolution of certain metal ions, whereas higher pH values could lead to their precipitation, thereby influencing the concentration of components during the freeze concentration process³⁰. Furthermore, pH changes can alter the reaction rates of chemical processes in thermal spring water, subsequently affecting the distribution of therapeutic components. Additionally, therapeutic elements exhibit higher bioactivity under specific pH conditions. Therefore, pH regulation plays a critical role in enhancing the concentration efficiency of therapeutic components in thermal spring water. In this study, three pH gradients

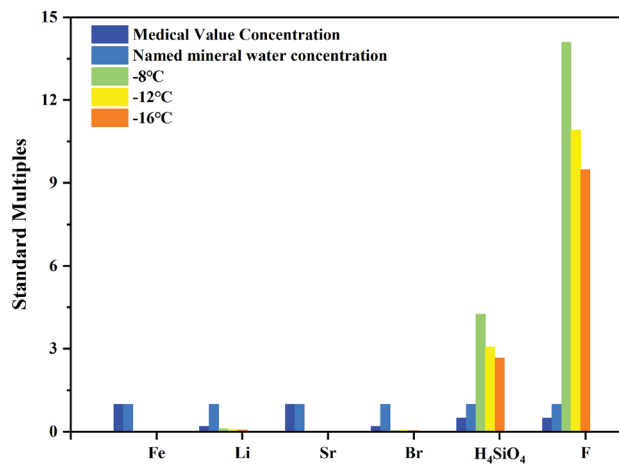


Fig. 7. Comparison of physiotherapeutic value components and standard values under the influence of freeze concentration temperature. Note: The “Medical Value Concentration” and “Named mineral water concentration” are both based on the Chinese national standard Classification and Evaluation Standard for Geothermal Water (GB11615-2010). The standard multiplier for the “naming mineral water concentration” is uniformly 1.0, while the multipliers for the “medical value concentration” are as follows: F: 0.5, H₄SiO₄: 0.5, Sr: 1.0, Li: 0.2, Br: 0.2, and Fe: 1.0. The corresponding concentration values are provided in Table S1, and this convention is used consistently throughout the manuscript.

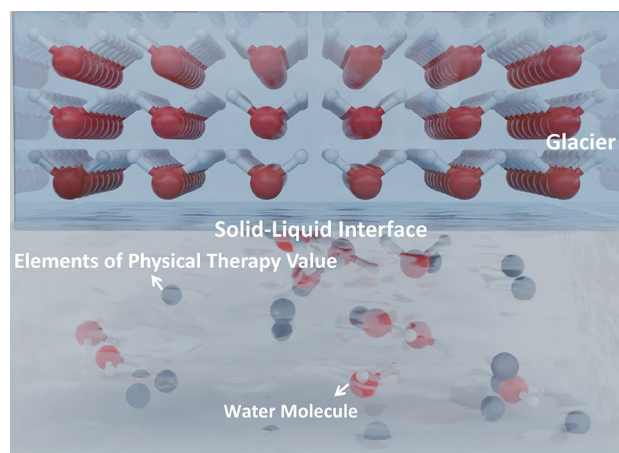


Fig. 8. Schematic diagram of freeze concentration.

were established (pH = 4, pH = 6, and pH = 8) to investigate the influence of pH on the freeze concentration of therapeutic components. The results are presented in Fig. 9.

The results indicate that at pH = 8, the concentration factors for Li, Sr, F, and H₄SiO₄ were 2.75, 1.76, 2.71, and 1.73, respectively. Throughout the concentration process, H₄SiO₄ exhibited a steady and uniform increase, whereas the increments for other therapeutic components were smaller compared to H₄SiO₄. The comparison of therapeutic components under freeze concentration influenced by pH and their standard values is shown in Fig. 10. After concentration, the levels of F and H₄SiO₄ reached 13.17 and 2.63 times their respective thresholds for thermal mineral water classification (Fig. 10). At pH = 6, Li increased to 0.41 mg/L, Sr to 0.11 mg/L, F to 26.35 mg/L, and H₄SiO₄ to 177.25 mg/L. During the entire concentration process, the increment of H₄SiO₄ was larger than that observed under the condition of pH = 8. After concentration, the levels of F and H₄SiO₄ reached 13.18 and 3.54 times their respective thresholds for thermal mineral water classification (Fig. 10). At pH = 4, the concentration factors for Li, Sr, F, and H₄SiO₄ were 2.50, 1.29, 2.27, and 1.86, respectively. After concentration, the levels of F and H₄SiO₄ reached 8.95 and 2.84 times their respective thresholds for thermal mineral water classification (Fig. 10).

Under pH conditions of 4 and 6, the pH value gradually increased during the concentration process, rising from 4.04 to 5.27 and from 5.99 to 7.47, respectively. In contrast, at pH = 8, the pH value gradually decreased, dropping slowly from 8.08 to approximately 7.9. The decrease in the initial pH facilitates the dissolution of metal cations in the thermal spring water, enhancing the initial concentrations of therapeutic components. Additionally, changes in pH influence the speciation of potentially toxic elements in the thermal water. In acidic environments,

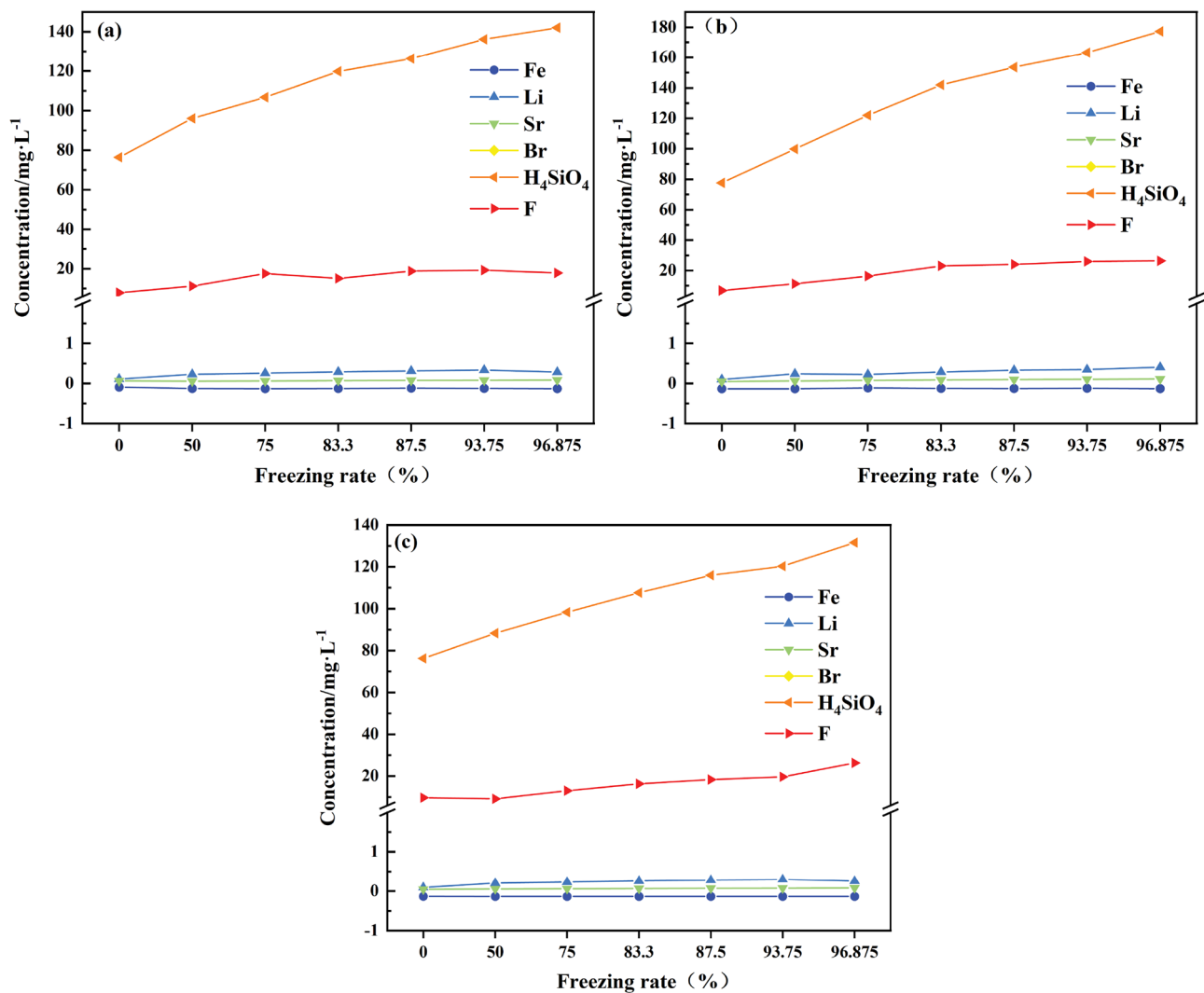


Fig. 9. Effect of pH value on freezing concentration of valuable elements of Lushan hot Spring physiotherapy: (a) pH 8; (b) pH 6; (c) pH 4.

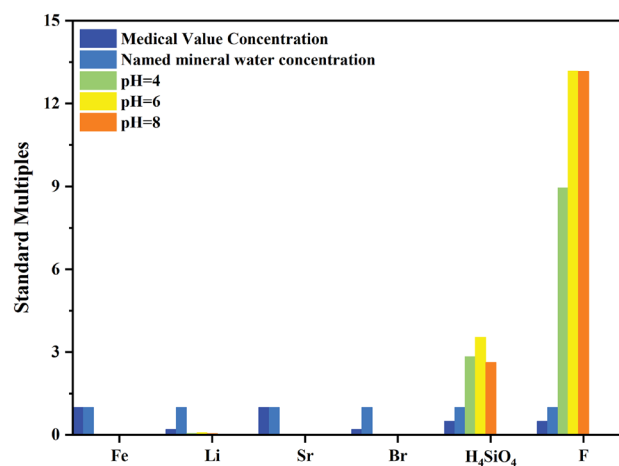


Fig. 10. Comparison of physiotherapeutic value components and standard values under the influence of frozen concentrated pH value.

therapeutic components in the thermal spring water primarily exist in highly mobile forms³¹. Based on the concentration performance of the therapeutic components, pH = 6 provided the optimal freeze concentration effect at the best freezing temperature. Adjusting the thermal spring water pH to 6 during freeze concentration is more conducive to concentrating therapeutic components. Li and Sr achieved a certain degree of concentration; however, the effectiveness was limited by the entrainment loss inherent in the freeze concentration process, preventing them from reaching therapeutic mineral water's medically significant concentrations.

Evolutionary characteristics of potentially toxic elements

Monitoring potentially toxic elements during the concentration of thermal spring water is crucial. As water evaporates or undergoes other physical and chemical methods of removal during the concentration process, the concentrations of other elements and dissolved minerals in the water will increase. These elements may react chemically or precipitate with other substances during concentration, and certain potentially toxic elements (such as lead, arsenic, cadmium, chromium, etc.) may accumulate in the water, further raising their concentrations. When their levels become too high, they can pose a potential threat to human health³². Therefore, it is essential to discuss the concentration of potentially toxic elements in thermal spring water under the optimal concentration conditions ($T = -8\text{ }^{\circ}\text{C}$, $\text{pH} = 6$), with the results shown in Fig. 11.

From the slopes of the curves shown in Fig. 11(a), there was no significant accumulation of potentially toxic elements as the ice formation rate increased. Overall, the concentration of Zn increased during the concentration process, while the concentration of Se decreased. The final concentrations of As, Cd, Cr, Cu, Mn, Ni, Pb, Se, and Zn were 0.037, 0.0011, 0.002, 0.005, 0.014, 0.003, 0.002, 0.002, and 0.057 mg/L, respectively. Compared to the “Sanitary Standard for Drinking Water”⁵ the concentration of As exceeded the limit value (0.01 mg/L), indicating that the concentrated thermal spring water was not suitable for direct consumption. A linear regression of As concentration during the freeze concentration process revealed a decreasing trend (Fig. 11(b)). Although As was not detected in the initial hot spring water, its concentration exceeded the regulatory limits during most stages of freeze concentration. This phenomenon can be attributed to the physicochemical behavior of arsenic during ice formation, where it remains predominantly in the unfrozen liquid phase due to phase separation, rather than being incorporated into the ice lattice. Consequently, arsenic becomes progressively enriched in the residual solution. Similar trends have been reported in previous studies, where potentially toxic elements tend to concentrate in the liquid phase during the freezing of natural waters. Notably, the arsenic concentration decreased below the standard limit when the ice formation rate reached 93.75%. No heavy metal element exceeded the standard, but the concentration of F in the concentrated thermal spring water exceeded 1.5 mg/L (exceeded the WHO (2022) guideline value of 1.5 mg/L), making it unsuitable for the production of drinking natural mineral water. According to the “Groundwater Quality Standards” (GB14848-2017, China), the concentrated thermal spring water after freeze concentration falls into Category IV, which is suitable for agricultural production and some industrial water use. This suggests that the discharge of concentrated thermal spring water has minimal environmental impact.

Study of atmospheric pressure evaporation concentration

Effect of temperature

The effects of temperature on the evaporation concentration of therapeutic components in Lushan hot spring water at atmospheric pressure are shown in Fig. 12. The results indicate that at $140\text{ }^{\circ}\text{C}$, the concentration factors for Li, Sr, F, Br, and H_4SiO_4 were 17.83, 6.40, 16.16, 3.79, and 14.06, respectively. After concentration, the F and H_4SiO_4 concentrations reached 66.74 and 20.63 times their respective named mineral water concentrations (Fig. 13), while the Li concentration reached 2.88 times the medically valuable concentration. At $120\text{ }^{\circ}\text{C}$, the concentration factors for Li, Sr, F, Br, and H_4SiO_4 were 12.14, 6.66, 16.16, 1.14, and 11.23, respectively. After concentration, the F and H_4SiO_4 concentrations reached 66.74 and 16.48 times the named mineral water

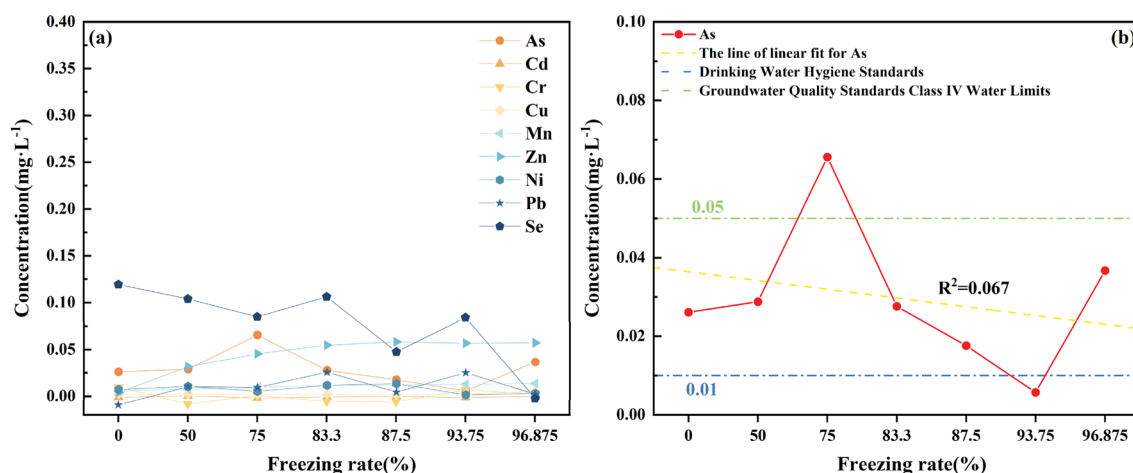


Fig. 11. Lushan hot spring potentially toxic elements freezing concentration process: (a) concentration variation curve; (b) linear fitting of the concentration distribution of As.

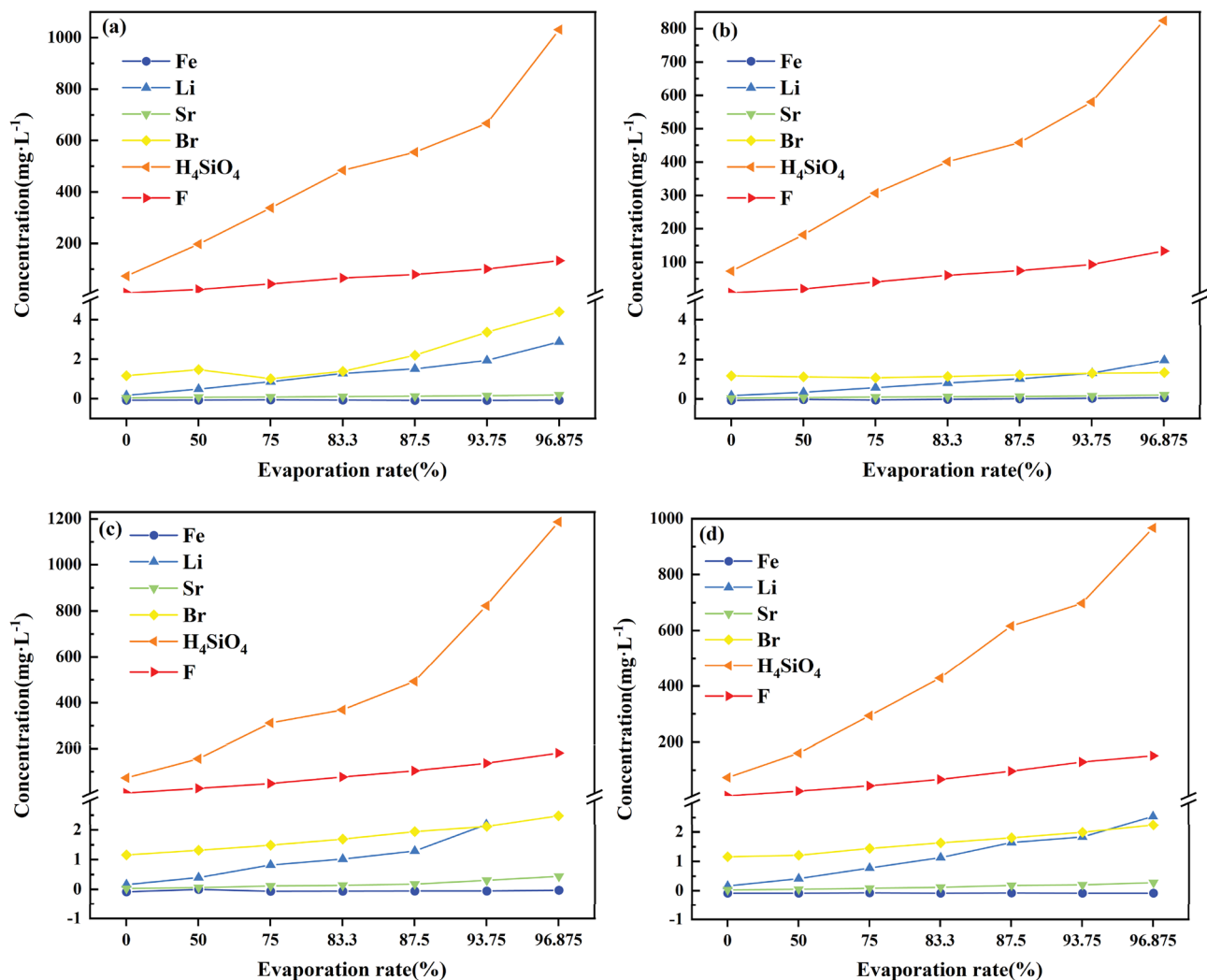


Fig. 12. Effect of temperature on atmospheric pressure evaporation concentration of valuable elements of Lushan hot Spring physiotherapy: (a) evaporation temperature 140 °C; (b) evaporation temperature 120 °C; (c) Evaporation temperature 100 °C; (d) Evaporation temperature 80 °C.

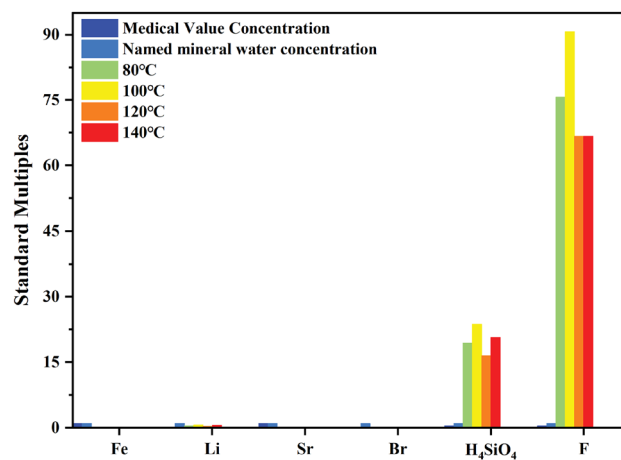


Fig. 13. Comparison of physiotherapeutic value components and standard values under the influence of atmospheric pressure evaporation concentration temperature.

concentrations, and the Li concentration reached 1.96 times the medically valuable concentration (Fig. 13). At 100 °C, Li increased from 0.16 mg/L to 3.14 mg/L, Sr from 0.03 mg/L to 2.48 mg/L, F from 7.54 mg/L to 181.50 mg/L, Br from 1.04 mg/L to 2.48 mg/L, and H_4SiO_4 from 73.38 mg/L to 1186.92 mg/L. After concentration, the F and H_4SiO_4 concentrations reached 90.75 and 23.74 times the named mineral water concentrations, while the Li concentration reached 2.48 times the medically valuable concentration (Fig. 13). At 80 °C, the concentration factors for Li, Sr, F, Br, and H_4SiO_4 were 15.72, 13.18, 9.50, 20.09, and 1.94, respectively. After concentration, the F and H_4SiO_4 concentrations reached 75.73 and 19.35 times the named mineral water concentrations, while the Li concentration reached 2.54 times the medically valuable concentration (Fig. 13).

During the atmospheric pressure evaporation concentration process, the concentration of HCO_3^- in the hot spring water increases as evaporation progresses and the water volume decreases, while some CO_2 is released. Additionally, a small amount of weak acidic components (such as silicates) gradually evaporates or is converted into volatile molecules, thereby reducing the proportion of acidic substances in the solution. This results in a gradual increase in pH, promoting the transformation of the solution toward alkalinity³³. The pH of the hot spring water increases during the reaction process, rising from an initial value of 8.72 to 9.42–9.76. Under atmospheric pressure, as the temperature increases, molecular movement intensifies, and the number of molecular collisions at the gas-liquid interface increases. With the continuous rise in thermal energy, when the kinetic energy exceeds the intermolecular attractive forces in the liquid, molecules can escape from the liquid surface and enter the space. In this study, the concentration of therapeutic components at 100 °C showed the best results. This is because, when the temperature exceeds the boiling point of the solution, excessive heat leads to a decrease in heat transfer efficiency and causes elements to volatilize, resulting in a higher loss rate of therapeutic components in the hot spring water³⁴. Therefore, 100 °C is the optimal temperature for atmospheric pressure evaporation concentration.

Effect of initial pH

The influence of pH on the atmospheric pressure evaporation concentration of therapeutic components in Lushan hot spring water is illustrated in Fig. 14. The results indicate that at pH 8, the concentration factors of Li, Sr, F, and H_4SiO_4 were 25.10, 4.05, 13.06, 3.49, and 13.26, respectively. After concentration, the concentrations of F and H_4SiO_4 reached 63.37 and 20.22 times the designated mineral water concentration, while the concentration of Li was 2.58 times the medically valuable concentration (Fig. 15). During the concentration process, the pH of the hot spring water increased from 8.08 to 9.54. At pH 6, the concentrations of Li, Sr, F, Br, and H_4SiO_4 were 2.50 mg/L, 0.59 mg/L, 121.10 mg/L, 1.42 mg/L, and 1037.50 mg/L, respectively. After concentration, the concentrations of F and H_4SiO_4 were 60.55 and 20.75 times the designated mineral water concentration, and the concentration of Li was 2.50 times the medically valuable concentration (Fig. 15). Throughout the concentration process, the pH increased from 5.99 to 7.98. At pH 4, the concentrations of Li, Sr, F, Br, and H_4SiO_4 increased from 0.11 mg/L to 4.32 mg/L, 0.07 mg/L to 0.71 mg/L, 7.90 mg/L to 143.25 mg/L, 1.16 mg/L to 1.28 mg/L, and 76.42 mg/L to 1784.82 mg/L, respectively. After concentration, the concentrations of F and H_4SiO_4 reached 71.63 and 35.70 times the designated mineral water concentration, and the concentration of Li reached 4.32 times the medically valuable concentration (Fig. 15). During the concentration process, the pH increased from 4.04 to 4.63.

At higher pH values (e.g., pH = 8), the solubility of certain metal ions in the solution decreases, making them more likely to precipitate. However, under lower pH conditions, some solutes are more readily dissociated into ionic forms, leading to an increase in solubility. Additionally, at lower pH, the higher concentration of H^+ ions in the solution facilitates the formation of stable complexes or ion pairs between H_4SiO_4 and F, thus preventing volatilization or precipitation losses³⁵. Based on the concentration factors of various therapeutic components, the atmospheric pressure evaporation concentration at pH 4 yields the best overall concentration effect, suggesting that adjusting the pH of the hot spring water to 4 during atmospheric pressure evaporation is more beneficial for concentrating the therapeutic value components.

Evolutionary characteristics of potentially toxic elements

Figure 16 shows the results of atmospheric pressure evaporation concentration of potentially toxic elements in the thermal spring water under optimal concentration conditions ($T = 100$ °C, $\text{pH} = 4$). The results indicate that Mn and Zn exhibited the most significant concentration effects. The final concentrations of As, Cd, Cr, Cu, Mn, Ni, Pb, Se, and Zn were 0.007, 0.003, 0.098, 0.139, 0.433, 0.062, 0.050, 0.128, and 0.600 mg/L, respectively. The concentrations of Cr, Mn, and Pb were above the maximum permissible limits defined by the guidelines of the World Health Organization (the maximum permissible limits are 0.05, 0.08, and 0.01 mg/L, respectively)⁵ while the concentrations of the other elements were generally below 0.2 mg/L. This suggests that the concentrated thermal spring water is not suitable for direct consumption due to potential health risks, but it still meets the standards for therapeutic mineral water and can be used for other purposes. Linear fitting of the concentration evolution of Cr, Mn, and Pb further reveals that Cr and Mn concentrations showed a rising trend during the concentration process. At the initial stage and at evaporation rates of 75% and 83.3%, Cr concentrations were below the standard, and at evaporation rates of 50% and 75%, Mn concentrations were also below the standard, indicating that these stages are safe and controllable. Pb, on the other hand, showed a decreasing trend, and its concentration was below the “Sanitary Standard for Drinking Water” at an evaporation rate of 93.75%, making it safe for use. Comparing the results with the “Drinking Natural Mineral Water” standard, the atmospheric pressure evaporation concentration results were consistent with the freezing concentration results. According to the “Groundwater Quality Standards,” the concentrated thermal spring water after atmospheric pressure evaporation falls into Category IV, which is suitable for agricultural production and certain industrial water uses, indicating that the discharge of concentrated thermal spring water has minimal environmental impact.

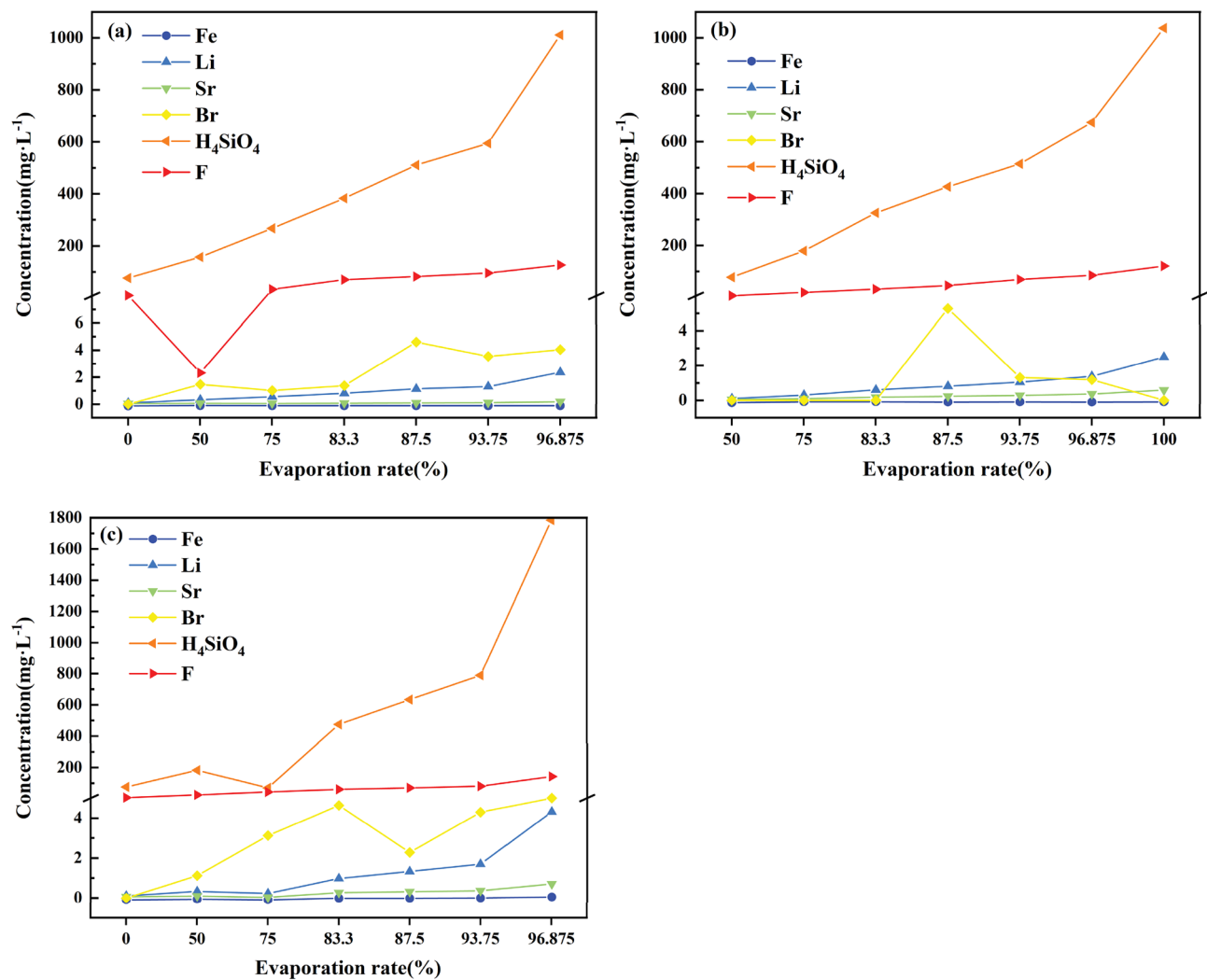


Fig. 14. Effect of pH value on atmospheric pressure evaporation concentration of valuable elements of Lushan hot spring physiotherapy: (a) pH 8; (b) pH 6; (c) pH 4.

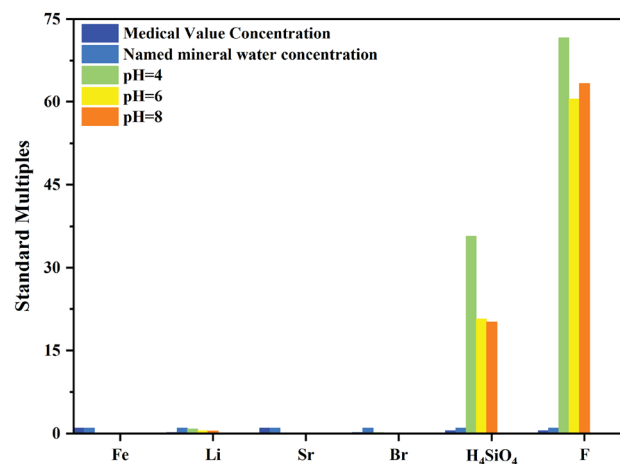


Fig. 15. Comparison of physiotherapeutic value components and standard values under the influence of atmospheric pressure evaporation concentration pH value.

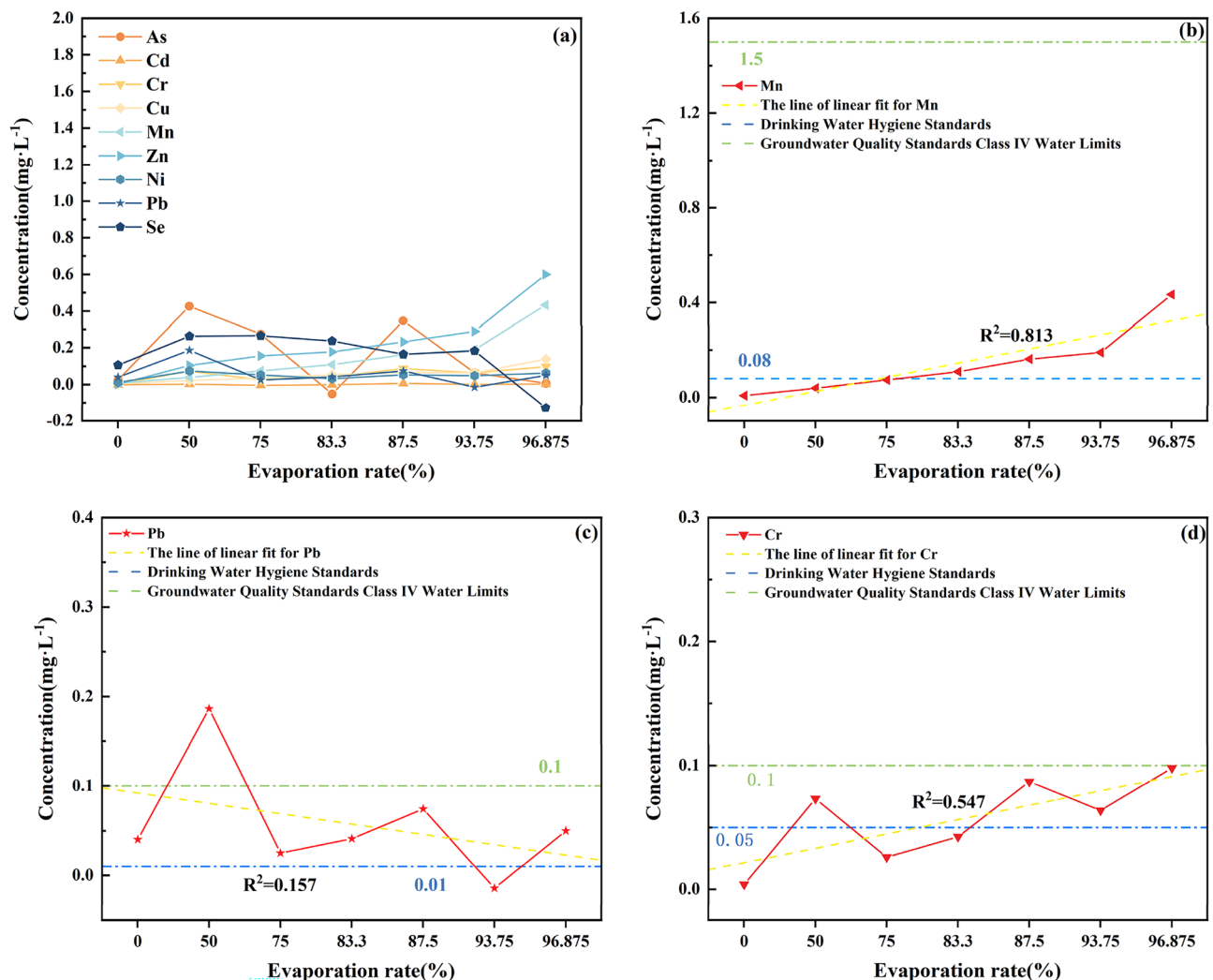


Fig. 16. Atmospheric evaporation and concentration of potentially toxic elements from Lushan hot Spring: (a) concentration variation curve; (b) linear fitting of the concentration distribution of Mn; (c) linear fitting of the concentration distribution of Pb; (d) linear fitting of the concentration distribution of Cr.

Differential analysis of enrichment technologies

Analysis of concentration effect

Figure 17 presents a comparison of the concentration coefficients of therapeutic components using different concentration techniques. As shown in the figure, under optimal conditions, the atmospheric pressure evaporation method exhibited the best concentration effect for the therapeutic components, with concentration coefficients for Li, Sr, Br, F, and H₄SiO₄ reaching 38.05, 10.68, 18.14, 4.58, and 23.36, respectively. In contrast, the freezing concentration method demonstrated inferior performance under optimal conditions, failing to achieve the expected results. The concentration coefficients for Li, Sr, F, and H₄SiO₄ were only 4.06, 2.33, 3.85, and 2.28, respectively, with Br showing little concentration due to its low initial concentration. The reasons for this can be attributed to two factors: firstly, the low concentration of therapeutic components in the thermal spring water resulted in limited solute availability during ice crystal growth and the resulting low solute concentration in the ice, leading to high solute entrapment in the ice crystals; secondly, the concentration gradient between the denser phase at the solid-liquid interface and the liquid phase was small, which, coupled with the low diffusion rate of molecules, meant that during the solute diffusion process, the solutes were easily “captured” by the growing ice crystals. Additionally, the low solute diffusion rate at lower temperatures led to a significant amount of solute being trapped in the ice or at its interface, preventing effective precipitation. Under these conditions, both the precipitation and enrichment efficiency of solutes were lower than those achieved by atmospheric pressure evaporation.

Analysis of energy consumption

(1) Energy Consumption Analysis of Freeze Concentration Method.

The theoretical energy consumption of the Lushan hot spring during the freeze concentration process includes the cooling energy consumption of the thermal spring water, phase change energy consumption, and

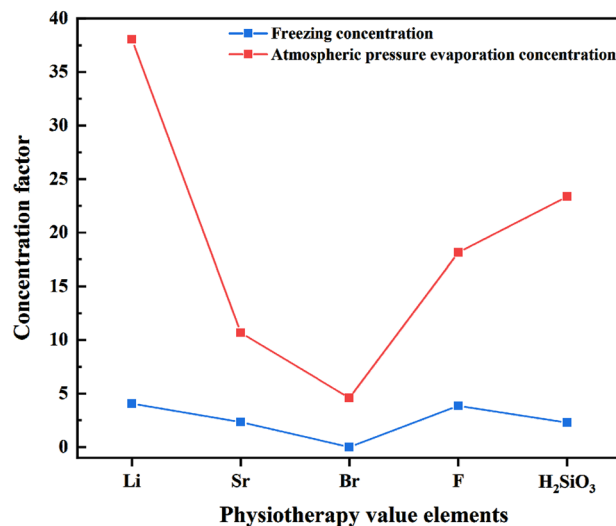


Fig. 17. Comparison of enrichment coefficient of physiotherapy value elements with different enrichment techniques.

the energy required to lower the temperature of the frozen thermal spring water to the specified temperature after freezing. In this energy consumption simulation, the designed treatment capacity of the Lushan hot spring for freeze concentration is 5 tons per day (based on the onsite flow rate of the thermal spring water), with an initial water temperature of 25 °C, a freezing temperature of −8 °C, and an ice formation rate of 95%. The calculation is shown in Formula 4³⁶:

$$Q = C_{wat}M\Delta t_1 + M\Delta_{fus}H \times 0.95 + C_{ice}M\Delta t_2 \times 0.95 \quad (4)$$

In the formula: Q : Required heat, kJ; C_{wat} : Specific heat capacity of thermal spring water, taken as $4.2 \times 10^3 \text{ J}/(\text{kg} \cdot ^\circ\text{C})$; M : Mass of thermal spring water, kg; Δt_1 : Temperature difference during cooling of thermal spring water, 25 °C; $\Delta_{fus}H$: Latent heat of fusion of ice, taken as 333.5 kJ/kg; C_{ice} : Specific heat capacity of ice, taken as $2.06 \times 10^3 \text{ J}/(\text{kg} \cdot ^\circ\text{C})$; Δt_2 : Temperature difference during cooling of ice, °C.

The electrical power required for the freeze concentration process is shown in Formula 5:

$$E = \frac{Q}{COP \times T} \quad (5)$$

In the formula: E : Required electrical power, kW; COP: Coefficient of performance, dimensionless; T : Operating time, in seconds.

In this simulation, the COP for the freeze concentration process was taken as 2.8³⁷. Under the design simulation conditions, the electrical power required for the Lu Mountain thermal spring freeze concentration process was calculated to be $E_{LP}=9.04 \text{ kW}$. The energy consumption using the freeze concentration method was determined to be 0.075kw·h/t. This energy consumption is based on theoretical calculations, and the actual energy consumption should be verified in specific engineering applications.

(2) Energy Consumption Analysis of Evaporation Concentration Method.

The theoretical energy consumption of the Lu Mountain thermal spring during the atmospheric pressure evaporation concentration process consists of two parts: (1) the energy required to heat the spring water, and (2) the phase change energy required for the vaporization of the spring water. In this energy consumption simulation, the design treatment capacity for the Lu Mountain thermal spring atmospheric pressure evaporation concentration process is 5 t/d, with the initial water temperature of 25 °C, evaporation temperature of 100 °C, and an evaporation rate of 95%. The calculation is shown in Eq. (6)^{38,39}:

$$Q = C_{wat}M\Delta t_1 + M\Delta_{vap}H \times 0.95 \quad (6)$$

In the above equation, $\Delta_{vap}H$ represents the latent heat of vaporization of water, which is taken as 2266 kJ/kg in this study.

In the energy consumption simulation, the coefficient of performance (COP) for the atmospheric pressure evaporation concentration is taken as 5.0⁴⁰. Under the design simulation conditions, the calculated electrical power required for the Lu Mountain thermal spring atmospheric pressure evaporation concentration process is $E_{CY}=28.56 \text{ kW}$, and the energy consumption for the atmospheric pressure evaporation method is 0.24kw·h/t. This energy consumption is based on theoretical calculations, and the actual energy consumption will need to be verified in specific engineering applications.

Based on the energy consumption analysis, it is evident that, although the freeze concentration method shows poor concentration effects for the therapeutic components of the Lu Mountain thermal spring, its efficiency is much higher than that of the atmospheric pressure evaporation concentration method, offering the advantage of low energy consumption. To address the limitations of the freeze concentration method, future approaches could involve initial concentration of therapeutic components using membrane filtration, followed by multi-stage freeze concentration to reduce carryover losses, thereby realizing the technical advantages of the freeze concentration method.

Analysis of the forms of therapeutic component species

The Lu Mountain thermal spring water contains various heavy metal ions, inorganic anions, and complexes. During the concentration process, the forms of therapeutic components change as a result of fluctuations in ion concentrations and water environmental parameters. In this study, PHREEQC was used to simulate the evolution of the forms of therapeutic components under two different concentration methods.

Table 6 presents the simulation results for the species of each component under the freeze concentration model. In the thermal spring, fluoride (F) predominantly exists as F^- , while lithium (Li) and strontium (Sr) are primarily found as Li^+ and Sr^{2+} , respectively, with their molar percentages exceeding 97%. Other species, such as $LiSO_4^-$, $LiCl$, $SrSO_4$, SrF^+ , and $SrCl^+$, are present in very low concentrations, indicating their negligible presence in the Lu Mountain thermal spring water. The molar percentage of F^- increases during the concentration process, while the proportion of HF decreases. This can be attributed to the continuous rise in pH during the concentration process, which enhances the concentration of F^- in the near-neutral to weakly alkaline environment, aligning with its concentration characteristics. Silicon (Si) predominantly exists as soluble SiO_2 , with a molar percentage exceeding 99%.

The Pourbaix Diagram can be used to determine the stable or predominant forms of elements under specific water chemical conditions⁴¹. All data were simulated using the PHREEQC software based on the `lnl.dat` thermodynamic database, and the diagrams were generated using visualization tools to ensure consistency and reliability in species distribution analysis. Figure 18 presents the Pourbaix diagram for the therapeutic value components under freeze concentration. The “▲” symbols represent the predominant species of the elements at the final stage of the freeze concentration process. From the diagram, it can be observed that Li^+ , Sr^{2+} , F^- , and soluble SiO_2 are the dominant forms for Li, Sr, F, and Si, respectively. These results are in close agreement with the PHREEQC simulation outcomes, indicating that under these conditions, these elements tend to form hydrated ions or soluble silicates. The dominant fields for Li^+ , Sr^{2+} , F^- , and soluble SiO_2 shift towards the negative axis of Eh as the pH increases. This suggests that in higher pH environments, these ions may react with hydroxide ions in the solution to form relatively stable hydrates or precipitates⁴².

Table 7 presents the simulation results for the species distribution under atmospheric evaporation concentration. In the thermal spring, F, Li, and Sr primarily exist in the forms of F^- , Li^+ , and Sr^{2+} , respectively. $SrSO_4$ and HF are the dominant secondary species for Sr and F, with their molar percentages reaching a peak at an evaporation rate of 87.5%, at 7.8784% and 6.6104%, respectively. As the pH increases, the mass percentage of $HSiO_3^-$ decreases, while the molar percentage of water-soluble SiO_2 remains above 99.9%.

Figure 19 presents the Eh-pH (Pourbaix) diagrams for therapeutic components under atmospheric evaporation conditions. From the diagram, it can be observed that Li^+ , Sr^{2+} , F^- , and soluble SiO_2 are the dominant species for Li, Sr, F, and Si, respectively, which is consistent with the PHREEQC simulation results. In Fig. 19(a), the dominant field of $LiHF_2$ appears, while in Fig. 19(d), the dominant field of SiF_6^{2-} increases compared to the freeze concentration method. Additionally, the areas of $H_2SiO_4^{2-}$ and $H_3SiO_4^-$ are smaller than those observed in the previous two methods. This indicates that under atmospheric evaporation conditions, the interaction between fluorides and metal ions is enhanced, while the dominant zones of silicon-containing components decrease due to changes in the concentration process.

During both freeze concentration and atmospheric evaporation concentration processes, the therapeutic value components in Lushan hot spring water, including F, Li^+ , Sr^{2+} , and soluble SiO_2 , retain their primary forms throughout the concentration process. As the concentration progresses, the molar percentage of these

components	Forms of existence	Concentration stage(%)			
		0	75	87.5	96.875
Li	Li^+	99.9306	99.9912	99.9790	99.9901
	$LiSO_4^-$	0.0904	0.0039	0.0083	0.0032
	$LiCl$	/	0.0049	0.0115	0.0067
Sr	Sr^{2+}	97.2805	99.7118	99.5483	99.6091
	$SrSO_4$	2.6611	0.1111	0.2219	0.0894
	SrF^+	0.0425	0.0977	0.1341	0.1528
	$SrCl^+$	0.0110	0.0786	0.1770	0.1053
F	F^-	99.8891	99.9884	99.9941	99.9962
	HF	0.1230	0.0093	0.0059	0.0038
Si	SiO_2	99.9922	99.9016	99.8827	99.7967
	$HSiO_3^-$	0.0078	0.0867	0.1375	0.2204

Table 6. Simulation results of freezing concentration form.

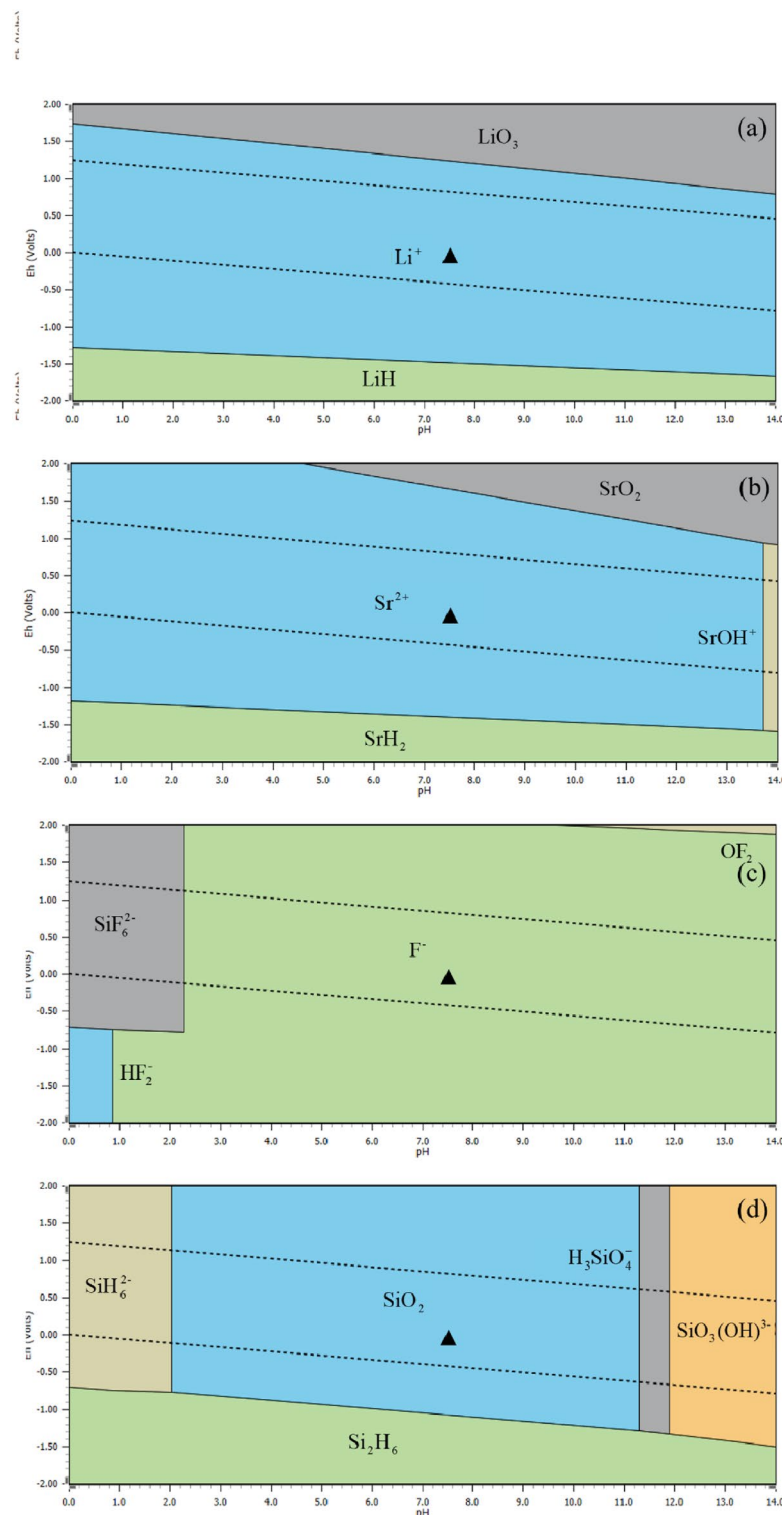


Fig. 18. Eh-pH dominance field of physiotherapy valuable components under freezing concentration: (a) Li; (b) Sr; (c) F; (d) Si.

components changes significantly, but they generally tend to form hydrated ions (such as Li^+ , Sr^{2+} , F^-) or soluble silicates (such as SiO_2). In the freeze concentration process, the increase in pH leads to a rise in the molar percentage of F^- , which may enhance the bioavailability of F^- in the hot spring water, contributing to improved therapeutic effects. Meanwhile, the concentration of SiO_2 promotes the formation of soluble silicates, which may, in some cases, enhance the therapeutic efficacy of the spring. However, the increase in SrSO_4 and HF

components	Forms of existence	Concentration stage(%)			
		0	75	87.5	96.875
Li	Li ⁺	99.9022	99.7321	99.4794	99.9038
	LiSO ₄ ⁻	0.0897	0.2400	0.4357	0.0889
	LiCl	0.0007	0.0394	0.0753	0.0137
Sr	Sr ²⁺	97.3219	93.9799	90.7526	96.9206
	SrSO ₄	2.6219	5.1467	7.8784	2.0554
	SrF ⁺	0.0499	0.2550	0.2877	0.8134
	SrCl ⁺	0.0123	0.6162	0.9211	0.2151
F	F ⁻	99.8488	95.1771	93.3762	95.7650
	HF	0.1487	4.8058	6.6104	4.2046
	FeF ⁺	0.0031	/	/	/
	HF ²⁻	0.0014	0.0031	0.0066	0.0083
	H ₂ F ₂	0.0001	0.0005	0.0017	0.0019
Si	SiO ₂	99.9841	99.9875	99.9055	99.9991
	HSiO ₃ ⁻	0.0118	0.0125	0.0008	0.0009

Table 7. Morphological simulation results of atmospheric evaporation concentration.

concentrations may lead to the formation of precipitates, potentially affecting the clarity and overall water quality⁴³.

Analysis of concentrated precipitated solids

(1) SEM-EDS

Phase analysis is a valuable method for identifying the forms of various components in water, especially minerals and dissolved chemical species. During the concentration process of hot spring water, phase changes of elements can provide insights into the specific effects of concentration on water quality. In this study, phase analysis was conducted on solid samples obtained under the optimal conditions of two concentration methods. The results are as follows:

Figure 20 shows the SEM images of the solid precipitates obtained by different concentration methods. Figure 20(a) and Fig. 20(b) display that the solids after freeze concentration have a flaky and block-like structure, with closely packed particles and only small pores between them. Figure 20(c) and Fig. 20(d) indicate that the solids precipitated by atmospheric evaporation concentration are primarily small particles, with similar contact forms and pore structures. The different microstructures observed in the precipitates obtained from the two concentration methods suggest that the elemental composition and content of the solids differ between the two methods⁴⁴.

Figure 21 shows the EDS spectra of the solid precipitates obtained by different concentration methods. The solid precipitates from freeze concentration mainly consist of O (46.35%) and Ca (50.68%), indicating that the precipitates may primarily include calcium chloride, calcium carbonate, and calcium hydroxide. The solid precipitates from atmospheric evaporation concentration predominantly contain Na (71.82%), O (6.33%), Ca (11.11%), and Si (6.49%), suggesting that the form and composition of the precipitates are more diverse, with Na-based compounds being dominant. Additionally, the elemental percentages of Fe and Sr in the atmospheric evaporation concentration solids increased, with Fe at 0.21% and 2.57%, and Sr at 0.25% and 1.70%, respectively. This indicates that the atmospheric evaporation concentration method has a greater impact on the Fe and Sr content in the thermal spring concentrate compared to the freeze concentration method.

(2) XPS

Figure 22 shows the XPS spectra of the solid precipitates from thermal spring concentration. The major substances present in the precipitates from both concentration methods are consistent, primarily including Na, O, Se, C, Cl, Si, and Fe. The XPS spectrum for Cl shows peaks at 1304.0 eV, 270.0 eV, and 198.9 eV, while the XPS spectrum for O shows peaks at 979.7 eV and 531.8 eV. The O1s peak at 531.8 eV corresponds to LiOH. The XPS spectrum for Fe 2p shows a peak at 719.9 eV, while the Na 1s spectrum shows a peak at 1071.8 eV, and Na 2s shows a peak at 63.3 eV. The Sr 3d spectrum has a peak at 133.7 eV, and the Si 2p spectrum shows a peak at 103.5 eV⁴⁵. From the overall peak profiles, it is observed that the freeze concentration method results in fewer types and lower relative content of Na compounds but more efficiently precipitates heavy metal elements such as K and Ca. The K peak is observed at 305.5 eV, and the Ca peaks are seen at 346.6 eV, 347.1 eV, and 437.8 eV. These results are in agreement with the EDS spectra analysis.

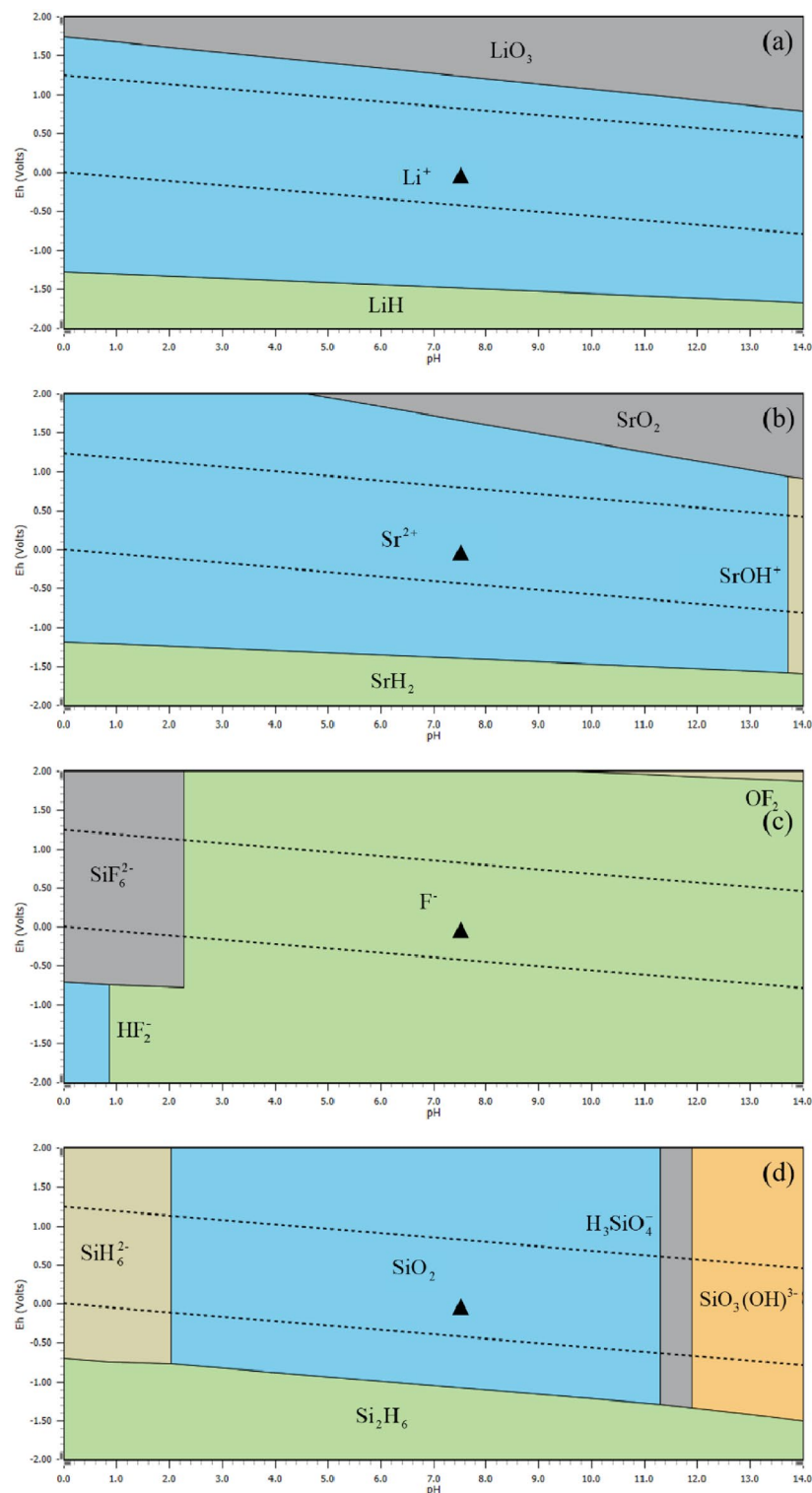


Fig. 19. Eh-pH dominant field of physiotherapy valuable components under atmospheric pressure evaporation concentration: (a) Li; (b) Sr; (c) F; (d) Si.

Conclusion

This study employed two concentration techniques—freeze concentration and atmospheric evaporation—to investigate the concentration behavior and enrichment characteristics of therapeutic components in Lushan geothermal water. The main conclusions are as follows:

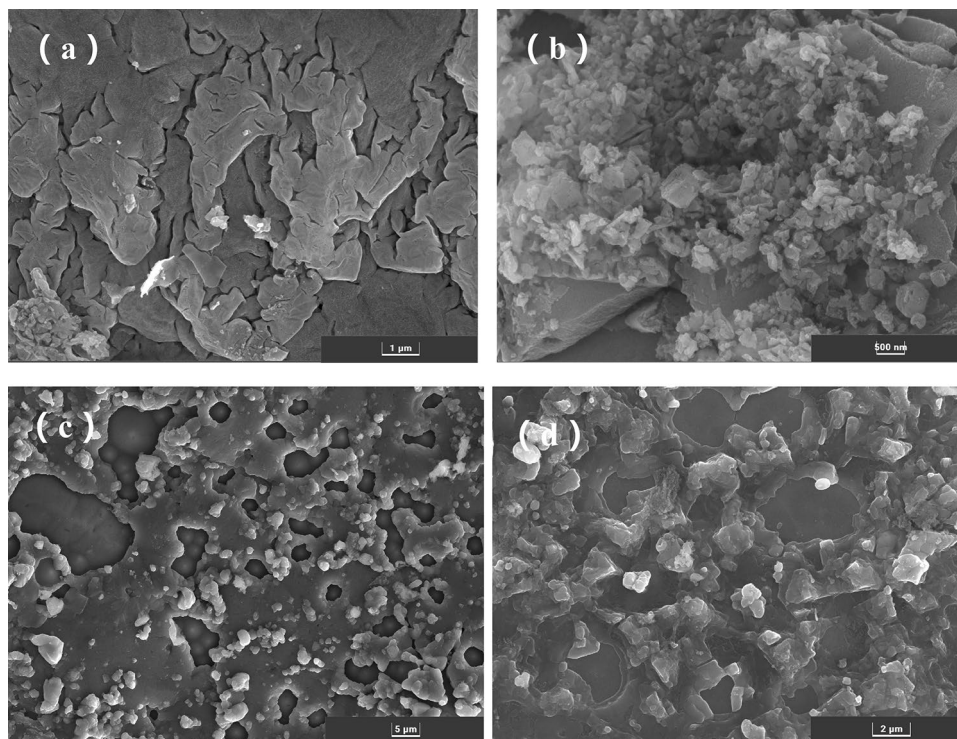


Fig. 20. SEM images of solids precipitated by different enrichment methods: (a)(b) freezing concentration; (c) (d) atmospheric concentration.

- (1) Both methods demonstrated varying degrees of effectiveness in enriching therapeutic components. Atmospheric evaporation at 100 °C and pH 4 achieved significant enrichment, with concentration factors for Li, Sr, Br, F, and H_4SiO_4 reaching 38.05, 10.68, 18.14, 4.58, and 23.36, respectively. Freeze concentration under −8 °C and pH 6 resulted in moderate enrichment, with concentration factors of 4.06 (Li), 2.33 (Sr), 3.85 (F), and 2.28 (H_4SiO_4). In both methods, the dominant chemical species (F^- , Li^+ , Sr^{2+} , and soluble SiO_2) remained stable throughout the concentration process.
- (2) During freeze concentration, the concentration of As decreased to below the safety threshold when the ice formation rate reached 93.75%. In atmospheric evaporation, Cr, Mn, and Pb exceeded standard limits at certain stages but ultimately remained within safe ranges. According to the Chinese Groundwater Quality Standard (GB 14848–2017), the concentrated waters from both methods fall under Category IV, making them suitable for agricultural and certain industrial uses, and indicating low environmental risk upon discharge.
- (3) The two concentration methods showed significant differences in energy consumption. Freeze concentration required lower energy input (0.075 kWh/t), significantly less than atmospheric evaporation (0.24 kWh/t), suggesting that freeze concentration is a more energy-efficient and sustainable approach with promising application potential.
- (4) SEM–EDS analysis revealed that freeze concentration mainly generated calcium-based precipitates, while atmospheric evaporation produced a wider variety of solids, primarily sodium-based compounds. Additionally, atmospheric evaporation had a more pronounced impact on Fe and Sr concentrations in the concentrate. XPS analysis confirmed that both methods produced precipitates with similar elemental compositions, although freeze concentration resulted in higher levels of heavy metal precipitation.

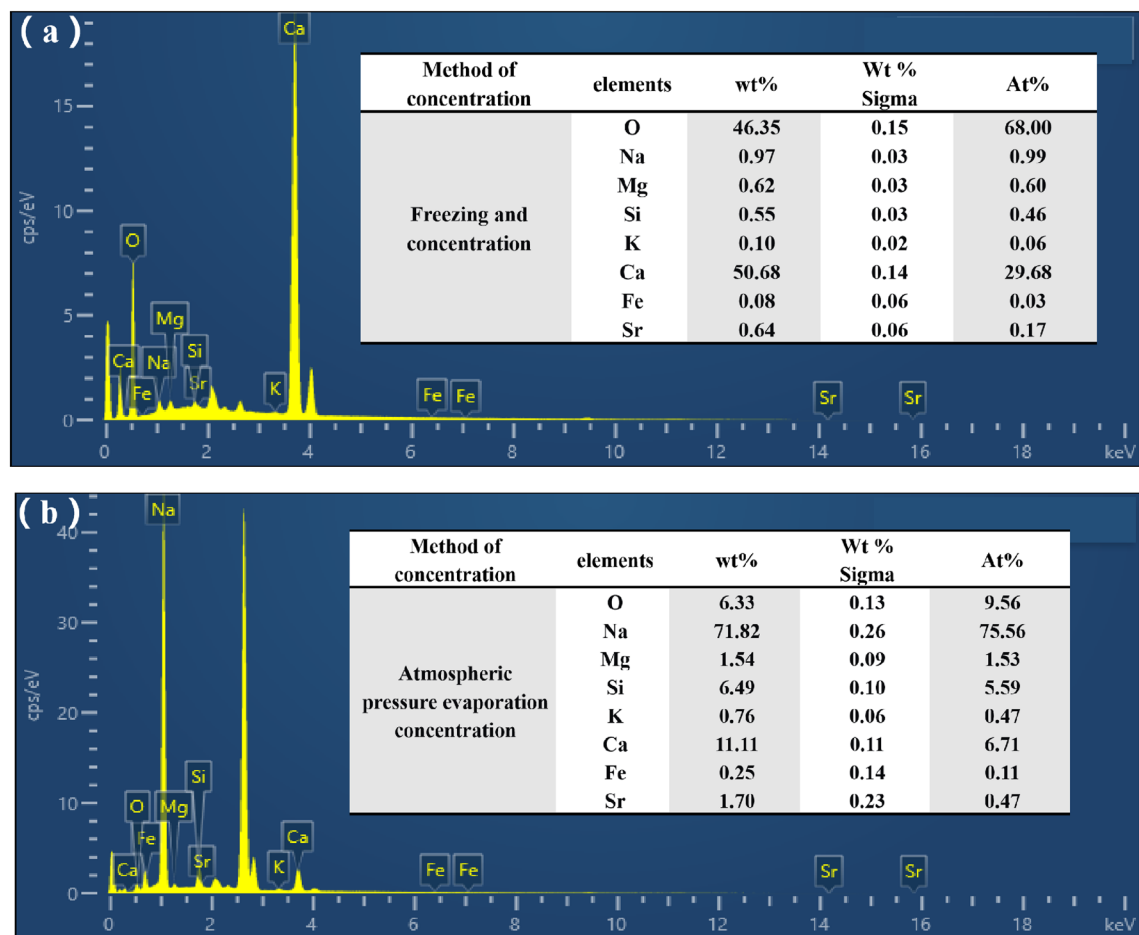


Fig. 21. EDS spectra of solids precipitated by different enrichment methods: (a) freezing concentration; (b) atmospheric evaporation concentration.

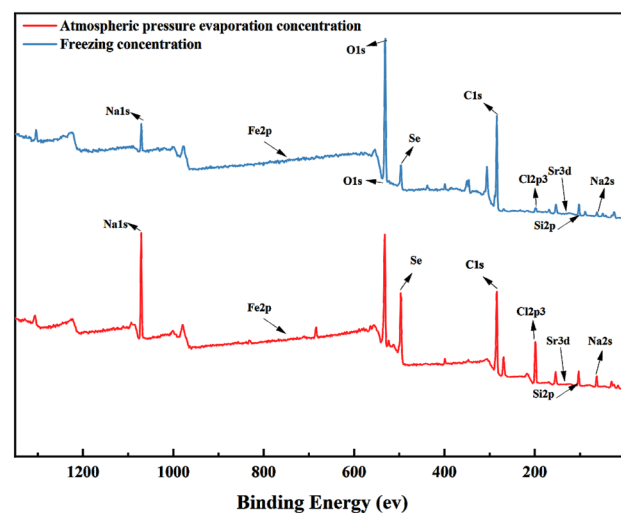


Fig. 22. XPS diagram of solid precipitated from hot spring concentration.

Data availability

The datasets generated during and/or analyzed during the current study are available from the corresponding author on reasonable request.

Received: 31 December 2024; Accepted: 11 June 2025

Published online: 01 July 2025

References

- Pentecost, A., Jones, B. & Renaut, R. W. What is a hot spring?. *Canadian J. Earth Sci.* **40**(11), 1443–1446 (2003).
- Kim, J. W. et al. Oct). THERAPEUTIC EFFECTS AND IMMUNOINFLAMMATORY REGULATION OF KOREAN HOT SPRING WATER. *J. Dermatol.* **41**, 16–16 (2014). <https://doi.org/10.1111/j.1396-9615.2014.00009.1>.
- Ngansom, W. & Duerrast, H. Assessment and ranking of hot springs sites representing geothermal resources in Southern Thailand using positive attitude factors. *Chiang Mai J. Sci.* **46** (3), 592–608 (2019). <https://doi.org/10.1016/j.jce.2019.03.001>.
- Chen, Z. S. et al. Classification of typical hot springs and their relationship with health in guizhou, China. *Environ. Geochem. Health.* **43** (3), 1287–1304. <https://doi.org/10.1007/s10653-020-00724-x> (2021, Mar).
- World Health Organization. Guidelines for drinking-water quality (4th ed., incorporating the 1st and 2nd addenda). Geneva: World Health Organization. (2022). <https://www.who.int/publications/i/item/9789240045064>
- Dey, R. K. et al. *Hydrogeochemical Processes Controlling the High Fluoride Concentration in Groundwater: a Case Study at the Boden Block Area, Orissa, India* 1843279–3291 (Environmental Monitoring & Assessment, 2012). 5.
- Wu, Y. Q. & Zhou, X. Source and influencing factors of metasilicic acid in mixed geothermal waters. *Geothermics* **123**, 103098. <https://doi.org/10.1016/j.geothermics.2024.103098> (2024, Nov).
- Zhang, T. D. W. W. Silicon isotope compositions of dissolved silicon and suspended matter in the Yangtze River, China. *Geochimica et Cosmochimica Acta.* (2004).
- Durowoju, O. S., Ekosse, G. I. E. & Odiyo, J. O. Occurrence and Health-Risk assessment of trace metals in geothermal springs within soutpansberg, Limpopo province, South Africa. *Int. J. Environ. Res. Public Health.* **17** (12). <https://doi.org/10.3390/ijerph17124438> (2020, Jun). Article 4438.
- Farhat, N., Hussain, S., Faisal, F., Batool, I. & Noreen, M. Physico-chemical characteristics and therapeutic potential of Chutrun thermal springs in Shigar valley, Gilgit-Baltistan (Pakistan). *Appl. Water Sci.* **11** (2). <https://doi.org/10.1007/s13201-020-01354-5> (2021, Jan).
- Yang, B., Qin, Q. Z., Han, L. L., Lin, J. & Chen, Y. Spa therapy (balneotherapy) relieves mental stress, sleep disorder, and general health problems in sub-healthy people. *Int. J. Biometeorol.* **62** (2), 261–272. <https://doi.org/10.1007/s00484-017-1447-5> (2018, Feb).
- Wangchuk, P. et al. Jan). Water-Based therapies of bhutan: current practices and the recorded clinical evidence of balneotherapy. *Water* **13** (1). <https://doi.org/10.3390/w13010009> (2021). Article 9.
- Sheng, L. L. et al. Jan). A novel hot spring-mimetic hydrogel with excellent angiogenic properties for chronic wound healing. *Biomaterials* **264** <https://doi.org/10.1016/j.biomaterials.2020.120414> (2021). Article 120414.
- Choi, M. G. & Kim, J. H. Effect of drying methods on removal of residual solvents from solvent-induced amorphous Paclitaxel. *Korean J. Chem. Eng.* **34** (12), 3041–3047. <https://doi.org/10.1007/s11814-017-0252-5> (2017, Dec).
- Wang, L. P. Boron removal and its concentration in aqueous solution through progressive freeze concentration. *Environ. Technol.* **38** (17), 2224–2232. <https://doi.org/10.1080/09593330.2016.1255663> (2017).
- Zhang, Y., Zhang, L. Y. & Chen, G. Far Infrared-assisted sample extraction and solvent removal for capillary electrophoretic determination of the bioactive constituents in citri reticulatae Pericarpium. *Curr. Pharm. Anal.* **17** (1), 57–66. <https://doi.org/10.2174/1573412915666190523115607> (2021).
- Orellana-Palma, P. et al. Influence of cryoconcentration on quality attributes of Apple juice (*Malus domestica* Cv. Red Fuji) *Appl. Sci.* **10** (3), 959. <https://doi.org/10.3390/app10030959> (2020).
- Alizadeh, H. R., Mortezapour, H., Akhavan, H. R. & Balvardi, M. Physicochemical changes of barberry juice concentrated by liquid desiccant-assisted solar system and conventional methods during the evaporation process. *J. Food Sci. Technology-Mysore.* **58** (11), 4370–4381. <https://doi.org/10.1007/s13197-020-04919-z> (2021, Nov).
- Sir, M., Honzajková, Z. & TREATMENT OF MUNICIPAL LANDFILL LEACHATE BY THE PROCESS OF REVERSE OSMOSIS AND EVAPORATION. *Fresenius Environmental Bulletin*, 24(6A), 2245–2250. <https://doi.org/10.1007/s10653-020-00724-x> (2015).
- Tomaszewska, B. & Szczepański, A. Possibilities for the efficient utilisation of spent geothermal waters. *Environ. Ence Pollution Res.* **21** (19), 11409–11417 (2014).
- Shvartsev, S. L. et al. Geochemistry of the thermal waters in Jiangxi province, China. *Appl. Geochem.* **96**, 113–130. <https://doi.org/10.1016/j.apgeochem.2018.06.010> (2018, Sep).
- Shvartsev, S. L., Zippa, E. V. & Borzenko, S. V. Feb). The nature of low salinity and composition peculiarities of thermal waters in Jiangxi Province (China). *Russ. Geol. Geophys.* **61** (2), 196–213. <https://doi.org/10.15372/rgg2019105> (2020).
- Baird, R. B., Eaton, A. D. & Rice, E. W. *Standard Methods for Examination of Water and Wastewater* 23rd edn (American Public Health Association, American Water Works Association, Water Environment Federation, 2017).
- Yongyi, L. et al. Exploration of the borderline value of mineral evolution and precipitation based on Phreeqc simulation in uranium leaching process. *Nonferrous Met. Eng.*, **14**(11) 154–166 (2024).
- Son, C. & Lim, S. May). Control of Si₃N₄ etching kinetics and selectivity to SiO₂ by the additives in superheated water. *Ecs J. Solid State Sci. Technol.* **8** (4), N85–N91. <https://doi.org/10.1149/2.0161904jss> (2019).
- Hrdinka, T., Vlasák, P., Havel, L. & Mlejnská, E. Possible impacts of climate change on water quality in streams of the Czech Republic. *Hydrol. Sci. Journal-Journal Des. Sci. Hydrol.* **60** (2), 192–201. <https://doi.org/10.1080/02626667.2014.889830> (2015, Feb).
- Schroeder, W. F., Williams, R. J. J., Hoppe, C. E. & Romeo, H. E. Unidirectional freezing as a tool for tailoring air permeability in macroporous poly(ethylene glycol)-based cross-linked networks. *J. Mater. Sci.* **52** (23), 13669–13680. <https://doi.org/10.1007/s10853-017-1460-4> (2017, Dec).
- Shum, E. & Papangelakis, V. Water recovery from inorganic solutions via natural freezing and melting. *J. Water Process. Eng.* **31**, 100787. <https://doi.org/10.1016/j.jwpe.2019.100787> (2019, Oct).
- Liu, T. S. et al. Apr). Application of progressive freeze concentration in the removal of Ca²⁺ from wastewater. *J. Water Process. Eng.* **46**, 102619. <https://doi.org/10.1016/j.jwpe.2022.102619> (2022).
- Zhang, N., Huang, H. D., Yang, R. X., Zheng, A. L. & Moment, A. Aqueous metal ion leaching processes from high sulfur coal fly Ash for carbon mineralization: the importance of pH control on cation extraction, carbonate purity, and silicon Q structure. *Chem. Eng. J.* **474**, 145968. <https://doi.org/10.1016/j.cej.2023.145968> (2023, Oct).
- Fukuda, Y., Harada, M. & Okada, T. Jan). Adsorption/Desorption characteristics of metal ions on ferric oxyhydroxide during a Freeze-Thaw cycle. *Acs Earth Space Chem.* **8** (2), 263–273. <https://doi.org/10.1021/acsearthspacechem.3c00270> (2024).
- Le, T. V. & Nguyen, B. T. Heavy metal pollution in surface water bodies in provincial Khanh hoa, vietnam: pollution and human health risk assessment, source quantification, and implications for sustainable management and development. *Environ. Pollut.* **343**, 123216. <https://doi.org/10.1016/j.envpol.2023.123216> (2024, Feb).
- Poos, T. & Varju, E. Review for convection based evaporation of open liquid surface and equations of evaporation rate. *Int. Commun. Heat Mass Transfer.* **157**, 107755. <https://doi.org/10.1016/j.icheatmasstransfer.2024.107755> (2024, Sep).
- Yagov, V. V., Zabirow, A. R., Kaban'kov, O. N. & Minko, M. V. Heat transfer during cooling of high temperature spheres in subcooled water at different pressures. *Int. J. Heat Mass Transf.* **110**, 219–230. <https://doi.org/10.1016/j.ijheatmasstransfer.2017.03.029> (2017, Jul).

35. Bragin, I. V., Chelnokov, G. A. & Kharitonova, N. A. (Nov). New Isotope-Geochemical data on the thermal waters of the Talskoe deposit (Magadan Oblast). *Russian J. Pac. Geol.* **15** (6), 602–609. <https://doi.org/10.1134/s1819714021060026> (2021).
36. Lu, Z. L. et al. Evaluation of effects of freezing pretreatment on the grindability, energy consumption and chemical composition of wheat straw. *Renew. Energy*. **151**, 21–29. <https://doi.org/10.1016/j.renene.2019.10.139> (2020, May).
37. Rane, M. V. & Uphade, D. B. (Oct). Heat pump for Energy-Efficient sugarcane juice freeze Pre-concentration. *Sugar Tech.* **20** (5), 591–598. <https://doi.org/10.1007/s12355-017-0580-0> (2018).
38. Sofizadeh, T., Khodaei, J., Darvishi, H., Behrooz-Khazaei, N. & Saba, M. K. Process parameters of microwave heating-assisted vacuum evaporation of tomato juice: quality, energy consumption, exergy performance, and kinetic processing. *J. Microw. Power Electromagn. Energy*. **57** (3), 203–218. <https://doi.org/10.1080/08327823.2023.2235551> (2023, Jul).
39. Tian, S. H. et al. (Aug). Case study for enhancing concentration of waste dilute sulfuric acid by microwave flash evaporation: modelling, heat transfer, energy consumption and process optimization. *Sep. Purif. Technol.* **318**, 123930. <https://doi.org/10.1016/j.seppur.2023.123930> (2023).
40. Li, Y. L., Wu, H., Liang, X. G., Rong, C. J. & Chen, H. C. Experimental study of waste concentration by mechanical vapor compression technology. *Desalination* **361**, 46–52. <https://doi.org/10.1016/j.desal.2015.01.036> (2015, Apr).
41. Marin, O. A., Ordonez, J. I., Gálvez, E. D. & Cisternas, L. A. Pourbaix diagrams for copper ores processing with seawater. *Physicochemical Probl. Mineral. Process.* **56** (4), 625–640. <https://doi.org/10.37190/ppmp/123407> (2020).
42. Vanhellemont, J. (Oct). SiO₂ precipitate composition in si, revisited: discussion closed? *Phys. Status Solidi-Rapid Res. Lett.* **9** (10), 597–602. <https://doi.org/10.1002/pssr.201510313> (2015).
43. Olea-Olea, S. et al. Understanding the processes in a historically relevant thermal and mineral spring water by using mixing and inverse geochemical models. *Environ. Geochem. Health.* **44** (7), 2301–2323. <https://doi.org/10.1007/s10653-021-01166-9> (2022, Jul).
44. Fujii, K. et al. Physical characterization of meso-Erythritol as a crystalline bulking agent for Freeze-Dried formulations. *Chem. Pharm. Bull.* **63** (5), 311–317. <https://doi.org/10.1248/cpb.c14-00692> (2015, May).
45. Suthagar, K., Shanthi, K. & Selvam, P. Hydrogenolysis of glycerol over silica-supported copper-nanocatalyst: effect of precipitating-agent and copper metal-loading. *Mol. Catal.* **458**, 307–316. <https://doi.org/10.1016/j.mcat.2017.11.035> (2018, Oct).

Acknowledgements

The authors are extremely thankful to the anonymous reviewers that work in this paper.

Author contributions

CRediT authorship contribution statement: Bo Zhang: Investigation, Writing-original draft. Zheng Fang: Investigation, Supervision. Keng Xuan: Supervision, Writing - review & editing. Wenjie Ma: Conceptualization, Investigation, Data curation, Funding acquisition. Bai Gao: Supervision, Investigation, Funding acquisition. Yuanyuan Liu: Investigation, Supervision. Dandan Huang: Investigation, Supervision. Silei Xie: Investigation, Supervision. Yan Ding: Investigation, Supervision.

Funding

This research work was financially supported by the National Natural Science Foundation of China (Grant No. 42272301), the National Natural Science Foundation of China (Grant No. 41362011), the Youth Science Foundation Project (Grant No. 42302293), the Science and Technology Program of Jiujiang City (S2021ZDYFG090), and the Xuncheng Talents Program of Jiujiang (JJXC2023028).

Declarations

Competing interests

The authors declare no competing interests.

Additional information

Supplementary Information The online version contains supplementary material available at <https://doi.org/10.1038/s41598-025-06837-6>.

Correspondence and requests for materials should be addressed to B.G.

Reprints and permissions information is available at www.nature.com/reprints.

Publisher's note Springer Nature remains neutral with regard to jurisdictional claims in published maps and institutional affiliations.

Open Access This article is licensed under a Creative Commons Attribution-NonCommercial-NoDerivatives 4.0 International License, which permits any non-commercial use, sharing, distribution and reproduction in any medium or format, as long as you give appropriate credit to the original author(s) and the source, provide a link to the Creative Commons licence, and indicate if you modified the licensed material. You do not have permission under this licence to share adapted material derived from this article or parts of it. The images or other third party material in this article are included in the article's Creative Commons licence, unless indicated otherwise in a credit line to the material. If material is not included in the article's Creative Commons licence and your intended use is not permitted by statutory regulation or exceeds the permitted use, you will need to obtain permission directly from the copyright holder. To view a copy of this licence, visit <http://creativecommons.org/licenses/by-nc-nd/4.0/>.

© The Author(s) 2025